Optimizing High-Frequency Vibroseis Data

by

Theresa Ruth Rademacker

B.S., Benedictine College, 2003

Submitted to the Department of
Geology and the Faculty of the
Graduate School of The University
of Kansas in partial fulfillment
of the requirements for the degree
of Master of Science.

2006

Advisory Committee

_____

Richard D. Miller, Chair

_____

Ross Black

_____

George Tsoflias

_____

Jianghai Xia

_____

for the Department

Date Defended _____

The Thesis Committee for Theresa R. Rademacker certifies
that this is the approved version of the following thesis:

Optimizing High-Frequency Vibroseis Data

Advisory Committee

_____

Richard D. Miller, Chair

_____

Ross Black

_____

George Tsoflias

_____

Jianghai Xia

Acknowledgements

I would like to acknowledge the efforts of my advisor, Rick Miller, for his generous mentoring, financial support, and never-ending patience. I would also like to thank my primary professors George Tsoflias and Ross Black for teaching me about the different methods and mathematical proofs of geophysics. My thanks goes to Jianghai Xia for his computer programming skills.

I would also like to thank the KGS crew for their support in executing my surveys. My appreciation goes to Brett Bennett for his electronic expertise, Joe Anderson for his labor skills and Brett Wedel for helping with the acquisition process. Also, thanks to John Sallas and Elmo Christiansen for their technical support. My thanks goes to my fellow graduate students, Jamie Lambrecht, Shelby Walters and Lindsay Mayer for being there for me during this labor-intensive process.

A heartfelt thanks to my family, especially my Mom and Dad, who always made me realize my strength when I thought I had none. My thanks to Andy for his patience, and to my friends who cheered me on. Love you guys.

Table of Contents

Abstract....1
Introduction....2
Pre-survey Provisions....6
I.) Equipment Setup....7
II.) Telemetry System Noise....15
III.) Accelerometer Noise....28
IV.) IVI Minivib I Engine Noise....36
V.) Summary for Pre-survey Provisions....40
Adams Campus Survey....41
I.) Geology....42
II.) Equipment and Acquisition....46
III.) Processing and results....53
A.) 0-255 Hz....54
B.) 200-500 Hz....61
C.) 200-300 Hz....67
D.) 300-400 Hz....70
E.) 400-500 Hz....73
F.) Geophone response....76
Conclusion....80
References....82
Appendix A....85
Appendix B....86

List of Figures

Figure 1. Wave reflection....5
Figure 2. The RTS Box located in the Gator....9
Figure 3. Equipment configuration in the IVI Minivib and the seismograph....10
Figure 4. The Dytran 3184 model located on the reaction mass and baseplate....11
Figure 5. Location of the Dytran 3184 model accelerometer on the reaction mass....12
Figure 6. Location of the Dytran 3184 model accelerometer on the baseplate....13
Figure 7. The Endevco 7703A-1000 accelerometer....14
Figure 8. IVI Minivib I on the University of Kansas, West Campus....19
Figure 9. Circular design of the IVI Minivib I baseplate....20
Figure 10. The direct measurement of the radio signal with the ground force....21
Figure 11. Close-up of the first 500 ms on the radio signal....22
Figure 12. A datum shifting program lines up the two traces, revealing that there is a 96% correlation....23
Figure 13. Amplitude vs. frequency graph of the radio signal, ground force and the cross-correlation....24
Figure 14. *(Left)* Correlation of the radio signal with the ground force. *(Right)* The amplitude vs. frequency graph illustrates the dropout at higher frequencies....25

Figure 15. *(Left)* Deconvolution of the radio signal with the ground force. *(Right)* The amplitude vs. frequency graph demonstrates how high frequencies are maintained 26
Figure 16. *(Left)* The wavelet is closer in appearance to a spike. *(Right)* Applying a time varying filter to the deconvolution eliminates noise in the radio mass.....27
Figure 17. Background noise recorded at the baseplate and reaction mass 29
Figure 18. Amplitude difference for the baseplate accelerometer between a typical sweep to background noise.....30
Figure 19. Amplitude difference for the reaction mass accelerometer between a typical sweep to background noise.....31
Figure 20. Amplitude difference for the Endevco model baseplate accelerometer between a typical sweep to recorded background noise.....34
Figure 21. Background noise recorded with the engine set to 1800 rpm and with the engine off.....37
Figure 22. Noise generated from the engine as recorded on the frame.....39
Figure 23. Location and aerial photo of Adams Campus.....43
Figure 24. Location of Adams Campus and well Boehle 7 in Douglas County.....44
Figure 25. Gamma ray and neutron porosity log of well Boehle 7.....45
Figure 26. Two 28 Hz geophones buried underneath cement.....48
Figure 27. Schematic of the survey setup.....49
Figure 28. The five locations of the Endevco accelerometer.....50
Figure 29. Location of the survey on Adams Campus.....51
Figure 30. Photo of the geophone line.....52
Figure 31. Various geophone and accelerometer responses and synthetic sweep with a low bandpass filter (0-20-240-255).....56
Figure 32. Correlation of all configurations with the 28 Hz geophone (0-20-240-255)..57
Figure 33. Correlation of the different positions on the baseplate with the 28 Hz geophone (0-20-240-255).....58
Figure 34. Deconvolution with the 28 Hz buried geophone.....60
Figure 35. The frequency spectrum after deconvolution.....61
Figure 36. Various geophone and accelerometer responses and synthetic sweep with a 200-500 Hz frequency range.....62
Figure 37. Correlation of all configurations with the 28 Hz phone (200-500).....63
Figure 38. Correlation of the different positions on the baseplate with the 28 Hz geophone (200-500).....64
Figure 39. Deconvolution with the 28 Hz geophone for the 200-500 Hz frequency range.....65
Figure 40. The frequency spectrum after deconvolution.....66
Figure 41. Correlation of all configurations with the 28 Hz geophone (200-220-300-320).....68
Figure 42. Correlation of the different positions on the baseplate with the 28 Hz geophone (200-220-300-320).....69
Figure 43. Correlation of all configurations with the 28 Hz geophone (300-320-400-420).....71

Figure 44. Correlation of the different positions on the baseplate with the 28 Hz geophone (300-320-400-420).....72
Figure 45. Correlation of all configurations with the 28 Hz geophone (400-420-480-500).....74
Figure 46. Correlation of the different positions on the baseplate with the 28 Hz geophone (400-420-480-500).....75
Figure 47. The frequency spectra reveals how amplitude will die off with distance.....77
Figure 48. Graph depicting signal attenuation.....78
Figure 49. Deconvolution of the data set with the Endevco accelerometer at Position 4.....79

List of Tables

Table 1. Background and sweep amplitudes.....32
Table 2. Background and sweep amplitudes recorded for the Endevco model.....35
Table 3. Accelerometer measurements with the engine throttle set to 1800 rpm and with the engine off.....38

.

Abstract

Vibratory sources used for seismic investigation are often subjected to coupling and transmission problems between the baseplate and actuator mass system and the ground surface. This results in dramatic force amplitude fluctuations at points throughout the sweep and excessive attenuation of intermediate and higher frequencies ranging from 200 to 500 Hz. This study is focused on determining if the baseplate of a commercial high frequency hydraulic vibrator behaves like a rigid body throughout its operational frequencies. Specialty accelerometers were strategically placed to determine optimal location that best matches ground response as measured by a buried geophone. This aided in discovering aberations within the sweep spectra related to source configuration, and provided target enhancement opportunities for higher frequencies through optimized measurements of baseplate and ground coupling. The results show a significant variation in acceleration depending on where the accelerometer is positioned on the baseplate. Moreover, the baseplate accelerometer alone is sufficient for deconvolution.

Theresa Rademacker, M. S.

Department of Geology, 2006

University of Kansas

Introduction

Broadband minimum phase wavelets allow for the best seismic resolution and are necessary for optimal results on seismic reflection surveys (Hsueh and Mendel, 1983). Traditionally, vibroseis processing techniques have yielded a zero-phase Klauder wavelet produced through cross-correlation of the signal with the vibrator sweep (Brittle et al., 2001) (Appendix A). This process acts as a filter for frequencies that are outside the design spectrum of the seismic source. Phase variations associated with the Klauder wavelet are related to the acquisition characteristics, such as source performance coupling, reverberations, multiple reflections, and attenuation of higher frequencies (Futterman, 1962; Wuenschel, 1965; Robinson, 1967; Lines and Ulrych, 1977; Marschall and Knecht, 1986; Robinson and Treitel, 2000). Because cross-correlation is sensitive to slight variations in the propagated sweep away from the ideal, it is naturally prone to computational errors (Edelmann and Werner, 1982). An alternative method involves vibroseis deconvolution, which theoretically recovers the true reflectivities of the subsurface by removing the seismic source wavelet (Yilmaz, 1987). One advantage of using this technique is that for the ideal case, a broad frequency sweep would result in an accurate reflectivity spike.

Another matter to consider is the signal-to-noise ratio of source equipment used during acquisition. This includes the telemetry system used for transmission of the ground force, the accelerometers which measure the ground force, and engine noise from the vibrator. Deconvolution tolerates without signal degradation a certain threshold of environmental and processing noise, however extreme amounts can cause phase variations (Bickel, 1982).

Good coupling of the baseplate to the ground is essential for efficient energy transfer (Brittle et al., 2001). The source pulse continuously attenuates as the seismic wave propagates through the earth and reflects back to the surface (Figure 1) (Collins and Lee, 1956; Chapman et al., 1981). The amount of attenuation will differ depending on surficial characteristics including porosity, permeability (for sandstone) and clay content (Klimentos and McCann, 1990). By controlling the force output of the source relative to hold-down pressures, energy levels can be maintained that ensure decoupling does not occur (Sallas, 1984). Since the vibrator's force output is a function of physical motion of the baseplate (Appendix B), the baseplate's displacement, velocity and acceleration are known. If the baseplate ceases to act as a rigid body, then phase variations associated with machine specific baseplate flux will alter the transmitted seismic energy. Baseplate distortion can be detected through accelerometers placed on the baseplate. Comparisons of the ground force calculated using the various positions on the baseplate with recorded signal from a 28 Hz geophone buried in concrete below the baseplate allowed determination of specific accelerometer locations on the baseplate that more accurately represent the seismic waves going into the ground.

High resolution applications of reflection seismology continue to strive for increased imaging depths in the subsurface. In response to this need has come an increased demand for high-frequency vibroseis because it is non-invasive (Miller et al., 2004). To push dominant frequencies even higher (120 to 300 Hz), the vibrator must increase drive force. The ability and efficiency in delivering and recording high frequency energy to the ground is directly associated with the design of the vibratory source, therefore, electrical and mechanical modifications must be considered for

increasing resolution of standard vibroseis units, such as reducing plastic deformation and phase variations across the baseplate (Chapman et al., 1981). The high fidelity vibratory seismic (HFVS) method has produced significant improvements to seismic data using inversion phase minimum deconvolution (Allen et al., 1998), including improved wavelet stability, reduction of side lobe deformation and expansion of bandwidth. The HFVS method generally deals with situations in which there is more than one vibrator sweeping. For time/cost purposes, deconvolution is done in the field, so phase locking is important. The vibrator used for these experiments has no phase lock and is an open-loop circuit, meaning that the corrections to the ground force drive for location specific variations is developed based on the last sweep transmitted. The open-loop circuit is not a concern because deconvolution is not done in the field.

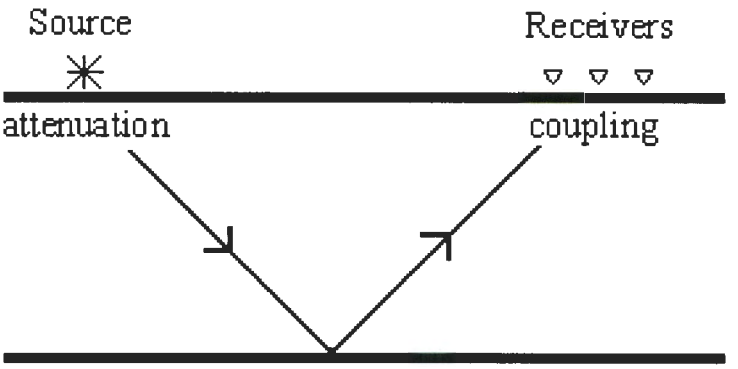


Figure 1. Wave Reflection (Chapman et al., 1981).

Pre-Survey Provisions

Noise interference can severely limit data quality. This includes environmental noise, such as traffic or wind, and noise within the recording equipment. Some recorded environmental noise can be controlled during a survey and edited out during processing (Klemperer and Brown, 1985), but noise within the recording equipment is usually overlooked and difficult to remove. Identifying and reducing noise in this source system could be effective in reducing problems associated with accurately isolating true ground force. Several potential contributors to background noise in source measurements include the telemetry system used for signal transmission, mass and baseplate accelerometers, and engine noise of the vibratory source. Locating and reducing the noise signature are essential aspects in deconvolving the ground force with the recorded sesimic signal and yield true reflectivity values (Bickel, 1982; Rademacker et al, 2005).

Equipment Setup

The equipment used during this study consists of a single vibrator and remote seismograph system that communicates via a Radio Trigger System (RTS) to the vibrator. Through a radio link, radio systems (in our case, the RTS-100) transmit or receive a trigger or vibrator reference signal and deliver that to the seismograph (IVI, 2006) (Figure 2). The equipment configuration allows the RTS located at the seismpgraph to send a start pulse to matched RTS box located in the vibrator, causing a trigger pulse that starts the vibrator controller, instructing the vibrator to sweep. Accelerometers located on the baseplate and reaction mass record the motion of the vibrator during a sweep. These measurements of acceleration travel through the Sytsem Interface Box (SIB), into the vibrator's controller where they are saved, through the RTS box again and sent back to the seismograph in analog form. The analog signal is then converted to digital form and recorded on the Geometrics Stratavisor NZC seismograph as a pilot trace (Figure 3) (IVI, 2006). The NZC seismograph has a built in anti-aliasing filter that is sensitive to the sampling rate and record time. For example, if a 10 s sweep of 20-500 Hz is produced and recorded with a sampling interval of 1 ms, the program will start filtering the signal around 83% of the Nyquist frequency, or at 415 Hz (Geometrics, 2006). The Nyquist frequency, f_{Nyq}, is calculated using the equation (Yilmaz, 2001):

$$f_{Nyq} = 1/(2\Delta t)$$

where Δt is the sampling interval. A sweep time of 5 s with a 0.5 ms sampling interval will avoid unwanted high frequency filtering within the critical portion of the bandwidth.

Two types of accelerometers were compared to appraise signal characteristic dependence. They were a Dytran model and Endevco model. Two Dytran 3184 accelerometers (Figure 4) are located on the Minivib I, with locations on the reaction mass (Figure 5) and baseplate (Figure 6). This model has a sensitivity level of 25 mV/g and was picked by IVI due to cost and available measurement range to reduce clipping of the signal.

The Endevco 7703A-1000 accelerometer was used based on an improved S/N ratio specification over the Dytran model. This accelerometer is driven by an external charge amplifier boosting signal strength. A sensitivity of 20 mV/g was used because it is very similar to the Dytran (Figure 7).

The recording system for this model is different than the Dytran. The Dytran models were directly connected to the computer system in the Minivib, whereas the Endevco model was hooked up to its own recording device (Geode and computer). This was done to allow all accelerometers outputs to be recording simultaneously during a sweep. The computer system recording the Endevco output allowed a self trigger, so the background noise could be recorded without generating a sweep.



Figure 2. RTS box used to transmit a trigger and receive a vibrator reference signal (IVI, 2006). This one is located in the Gator, a vehicle containing seismographs that allows access to remote areas. An identical RTS box is located in the IVI Minivib I.

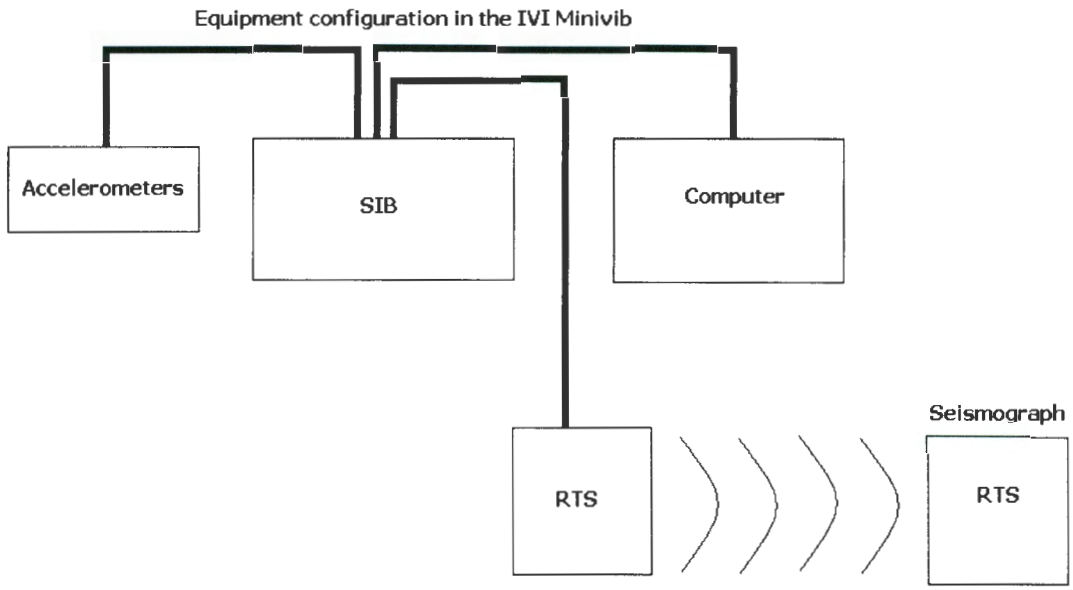


Figure 3. Equipment configuration in the IVI Minivib and the seismograph.



Figure 4. The Dytran 3184 model located on the reaction mass and baseplate. It has a sensitivity level of 25 mV/g.



Figure 5. Location of the Dytran 3184 model accelerometer on the reaction mass.

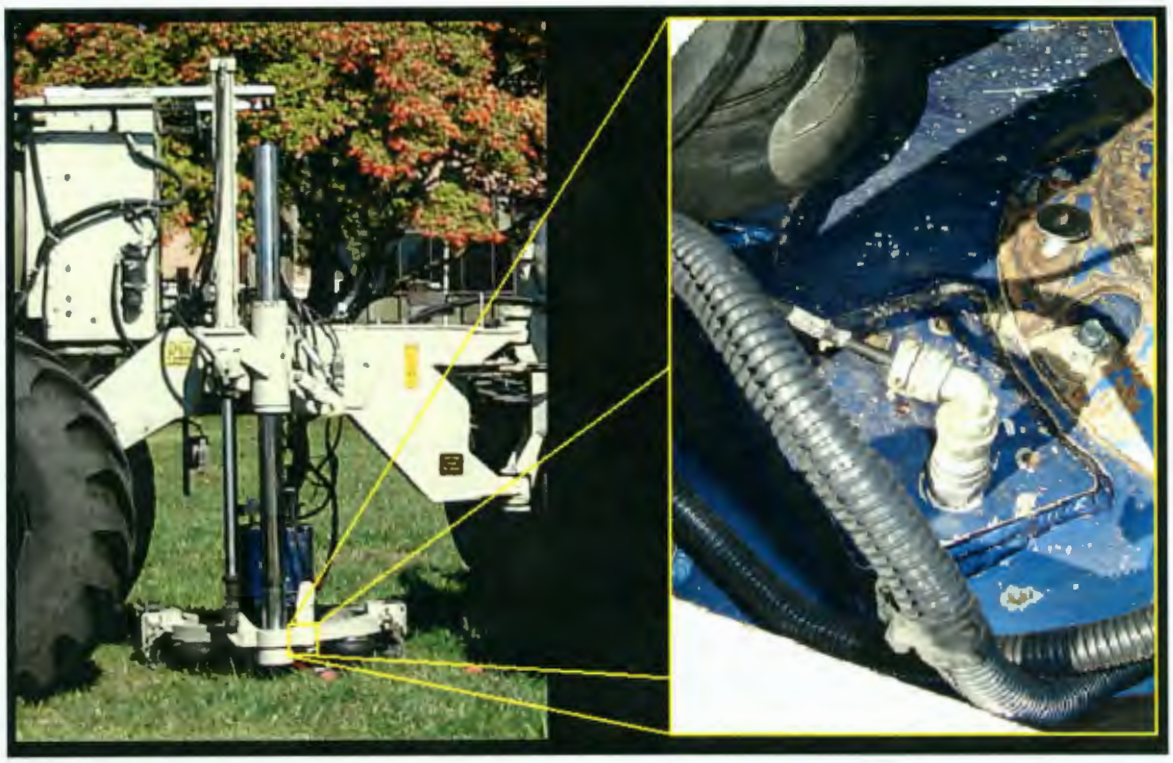


Figure 6. Location of the Dytran 3184 model accelerometer on the baseplate.



Figure 7. The Endevco 7703A-1000 accelerometer. When it is hooked up to the charge amplifier, it has a sensitivity of 20 mV/g.

Telemetry System Noise

This particular telemetry system reduces the possibility of radio interference associated with television, aircraft control towers and FM stations (http://www.hamuniverse.com/vhfuhfbands.html, 2006) by functioning in the ultrahigh frequency band. The telemetry system can transmit on two different frequency channels: 1457.525 MHz and 2457.9 MHz. One of three pilot signals can be transmitted: the ground force (GF), the filtered ground force (FGF) and the synthetic (SYN). The GF is a weight sum representation of the baseplate and reaction mass accelerometers theoretically yielding a true representation of the phase and amplitude transmitted for each sweep (Brittle et al., 2001). FGF is the GF with a high cut filter, and SYN delivers drive signal.

Radio noise needs to be quantifited because the transmitted reference signal is commonly used in wavelet compression routines. The Minivib I generated a 10 second, linear up-sweep with a frequency range of 20 to 250 Hz. Baseplate and reaction mass accelerometers recorded values used to calculate the ground force. The ground force was compared with the transmitted radio signal to reveal if noise is generated by the telemetry system. When no noise is present, the waveforms should be identical.

To determine this, the ground force is calculated using the equation (Baeten et al., 1990):

$$\text{Ground force} = m_b a_b + m_m a_m$$

The equation contains two known constants, baseplate mass, m_b and reaction mass, m_m. The IVI Minivib I (Figure 8) used for these experiments incorporates a circular baseplate design (Figure 9) with a mass, m_b, of 168 kg and a reaction mass, m_m,

of 141 kg. During a sweep, accelerometers located on the baseplate and reaction mass record values for a_b and a_m allowing calculation of the ground force.

Figure 10 shows the time difference between when the ground force is calculated and the radio signal is recorded. For the ground force, $t_0 = 0$ ms. On the radio signal, however, t_0 will be some time after the carrier wavelet starts transmission. The carrier noise is due to the radio frquency. Triggering of the RTS box initiates a start pulse that is transmitted for one RTS box to a second monitoring the selected band. The carrier wavelet is identifiable by the initial start pulse increase located at t = 160 ms (Figure 11). A datum shifting program reveals that the two traces match up with a 96% correlation (Figure 12). The other 4% is due to noise within the telemetry system.

Correlation of the two traces can determine the frequency amplitude output (Anstey, 1966). The convolutional model for a vibroseis seismic source is defined by the equation (Brittle et al., 2001):

$$x(t) = r(t)*s(t)$$

where x(t) is the recorded trace, r(t) is the reflectivity, s(t) represents the sweep, and all values are time dependent. * is the convolution operator. Collapsing the sweep into a source wavelet involves cross-correlation, $\otimes$, with the sweep:

$$x_{cc}(t) = r(t)*s(t)\otimes s(t) = r(t)*k(t)$$

where k(t) is the Klauder wavelet.

Amplitude spectra from correlation are dependent on the shape of the sweep (linear, nonlinear, Gaussian, etc.). This is different from deconvolution, where the amplitude spectrum is independent of sweep shape. When compared in the frequency domain, the amplitude spectra of the direct and telemetry ground force wave trains are

virtually identical. One would naturally assume that the correlation of these signals would show an excellent match, however, this is not the case. Considerable loss of signal within the high frequency portion of the correlated sweep is revealed on the telemetry trace (Figure 13). Correlation is done in the time domain so any time spectral variation will cause frequencies to destructively interfere and reduce amplitude. Along with this, a considerable amount of noise is seen (Figure 14).

On the other hand, deconvolution is performed in the frequency domain and therefore is independent of the shape of the sweep, such as whether it is linear or nonlinear, and taper values that change frequency amplitudes. This means that all the frequencies in the sweep are considered to have identical amplitudes (Figure 15).

The process of deconvolution is susceptible to noise enhancement, which is why it is crucial to identify it (Bickel, 1982). Noise is present in the radio signal at high frequencies from 180 to 250 Hz (Figure 15). A simple way to partially attenuate this noise is to apply a time varying filter that matches the sweep design. The filter does not remove noise at the same frequency and time as the sweep design. This filter was designed by examining the GF and determining the frequency range for a given time frame. Here is the time varying that was applied:

filter 1000 10 20 48 60
filter 2000 48 60 70 82
filter 3000 70 82 115 130
filter 4000 100 110 140 152
filter 5000 110 120 160 180
filter 6000 140 155 180 195
filter 7000 155 180 205 220
filter 8000 180 205 225 240
filter 9000 205 220 240 260

The first number in the line is the time that the filter will end, so for the first one, the filter will run from 0-1000 ms. For the next line, it will 1000-2000 ms, and so on. The last four numbers on each line construct the band pass that will run during that time frame. Figure 16 shows remarkable improvement to the deconvolved wavelet, bringing it closer to a spike. This begins to provide evidence as to how correlation provides less desirable results than deconvolution because resolution is improved.



Figure 8. IVI Minivib I on the University of Kansas, West Campus. This vehicle is the source of generating vibroseis seismic waves.



Figure 9. Circular design of the IVI Minivib I baseplate, which is 1018 in^2 with a radius of 18 in.

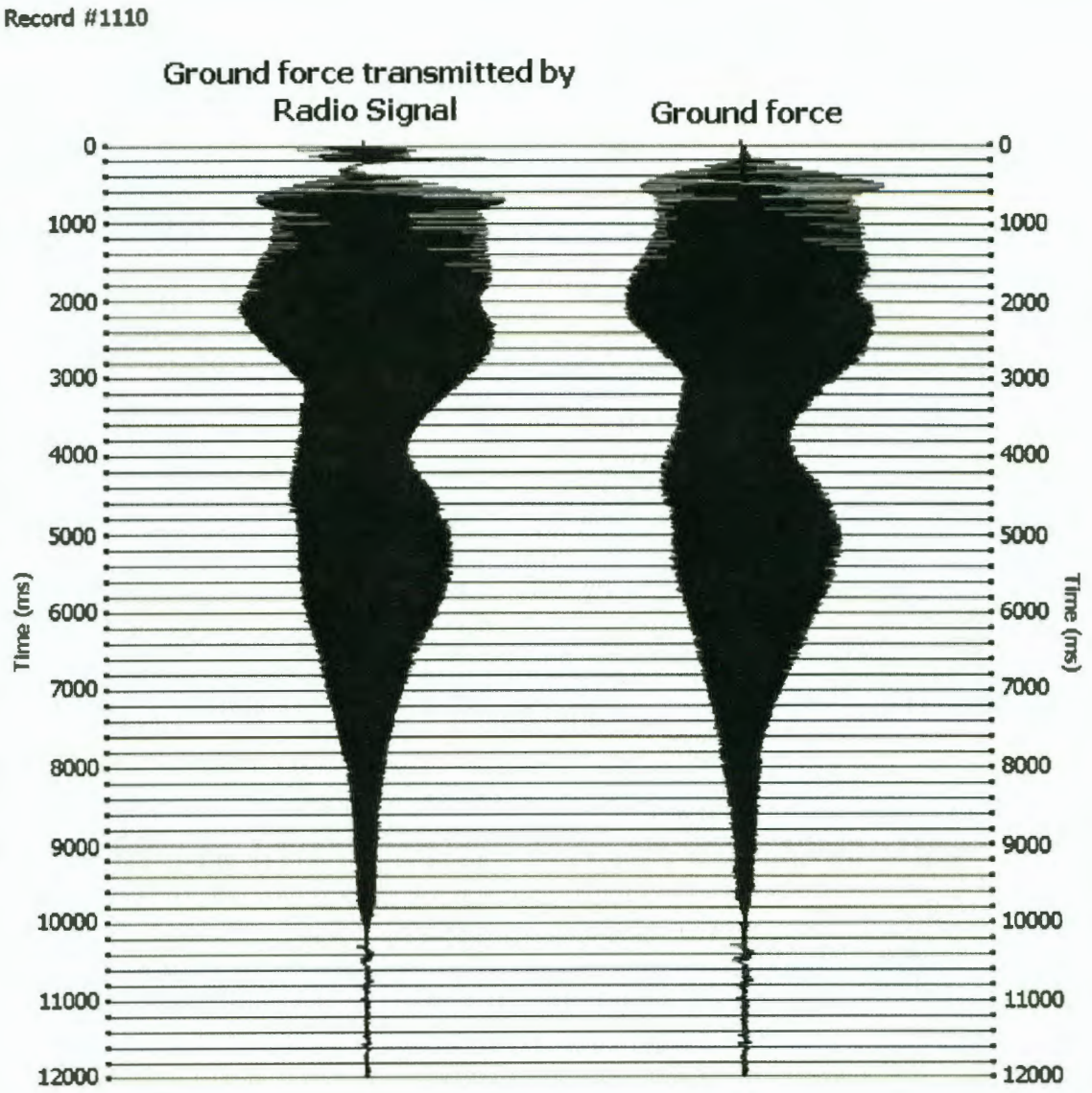


Figure 10. The direct measurement of the radio signal with the ground force. Arbitrary waveforms in the radio signal are located above the carrier wavelet at 160 ms.

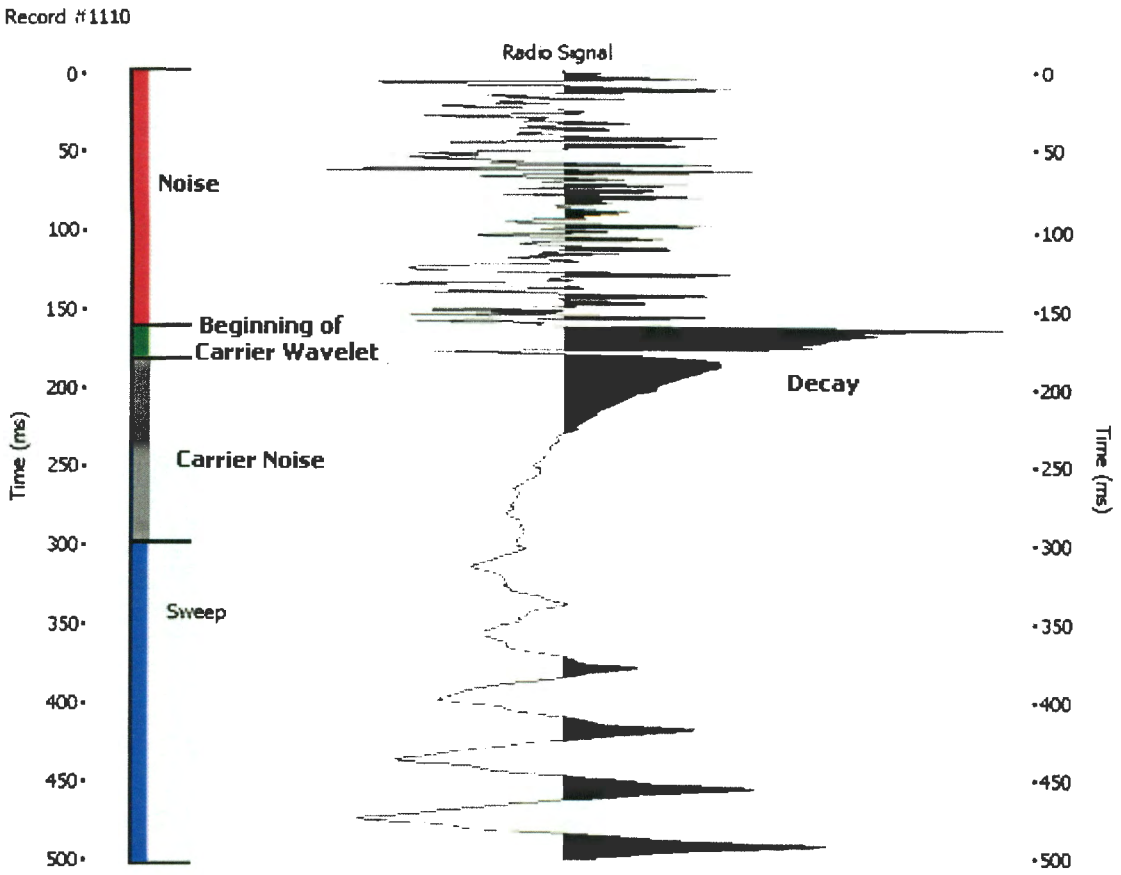


Figure 11. Close-up of the first 500 ms on the radio signal. Arbitrary noise begins at 0 ms and ends when the carrier wavelet starts at 160 ms and is characterized by a start pulse. It is not entirely clear where the carrier wavelet ends and the sweep begins.

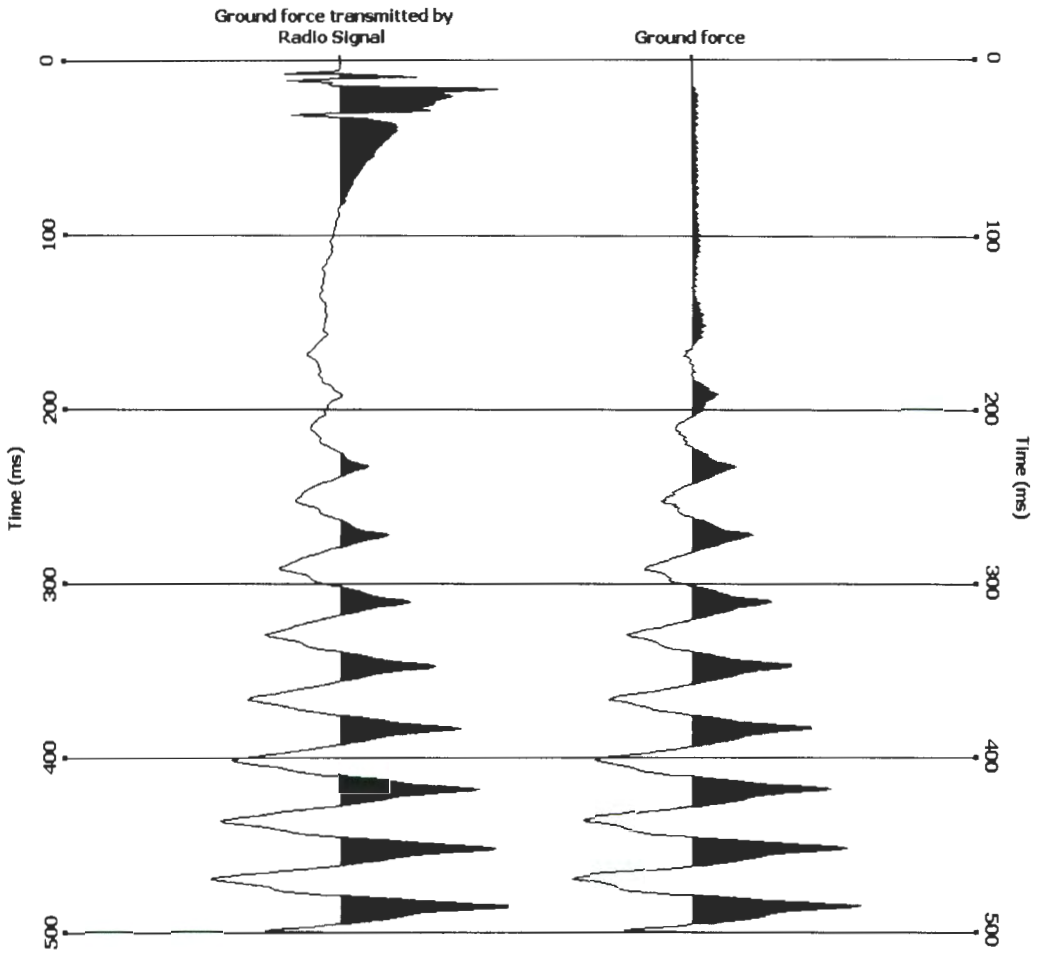


Figure 12. A datum shifting program lines up the two traces, revealing that there is a 96% correlation.

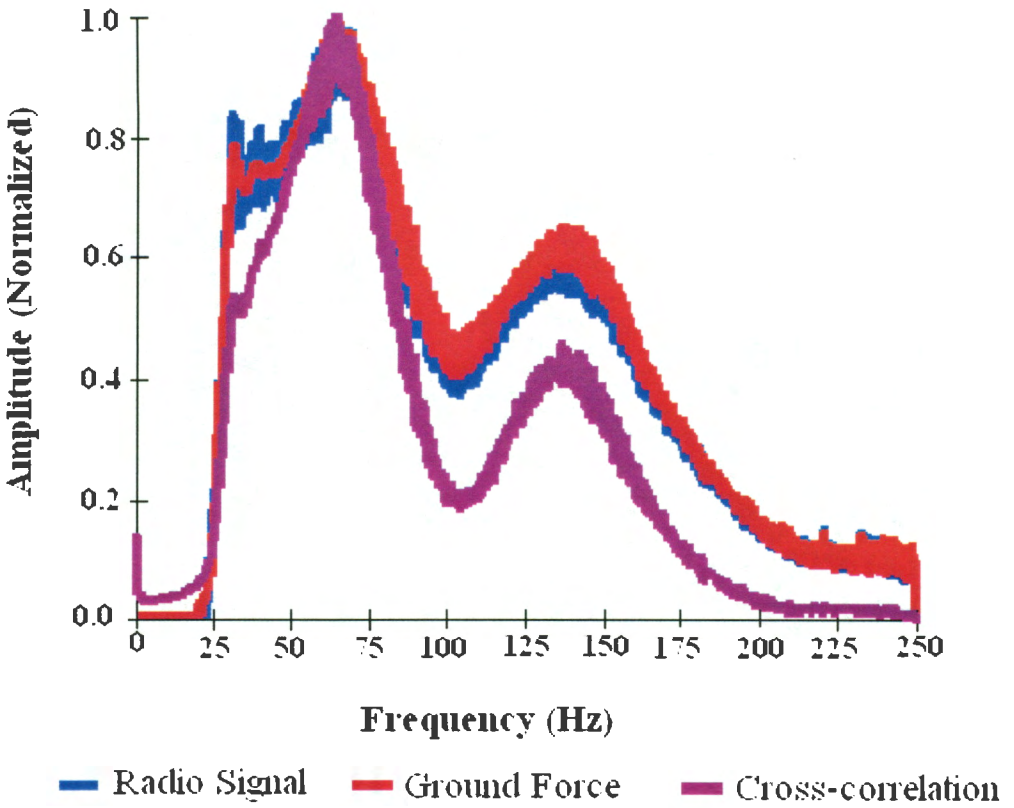


Figure 13. Amplitude vs. frequency graph of the radio signal, ground force and the cross-correlation. The radio and ground force are virtually identical. Correlation between the two reveals that there is a sizeable mismatch, particularly at high frequencies.

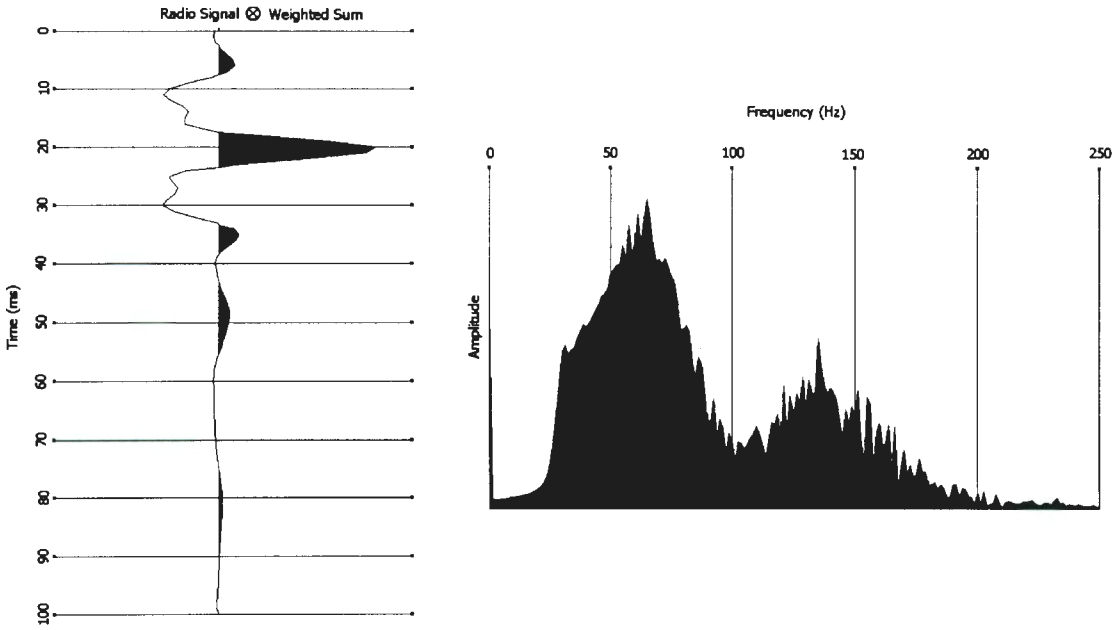


Figure 14. *(Left)* Correlation of the radio signal with the ground force. *(Right)* The amplitude vs. frequency graph illustrates the dropout at higher frequencies.

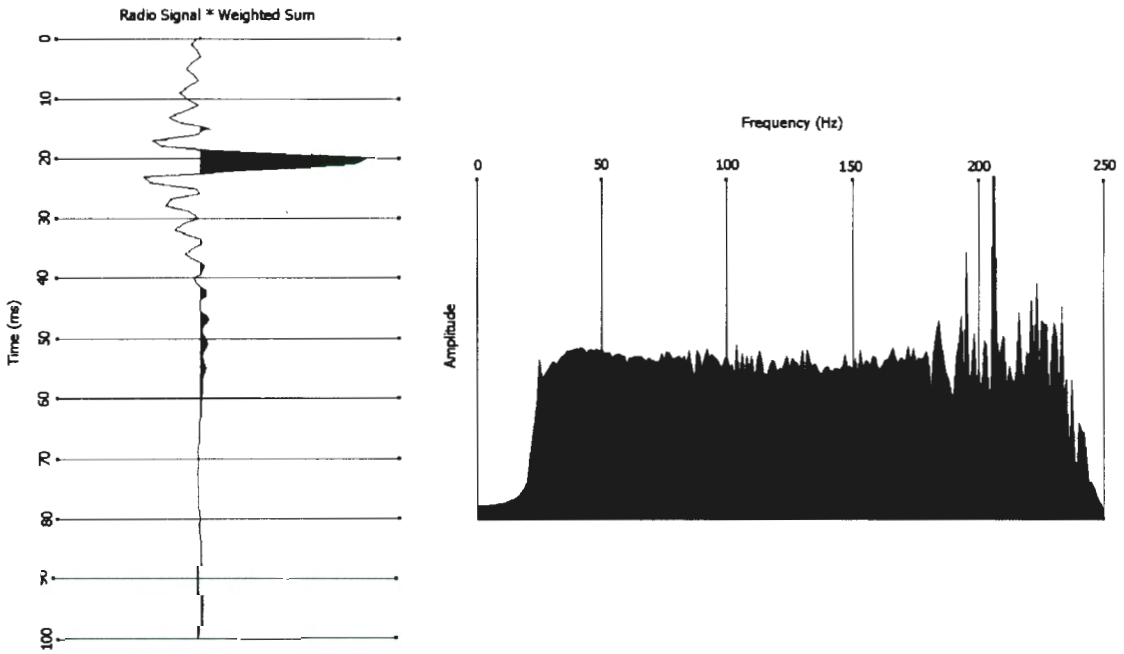


Figure 15. *(Left)* Deconvolution of the radio signal with the ground force. *(Right)* The amplitude vs. frequency graph demonstrates how high frequencies are maintained.

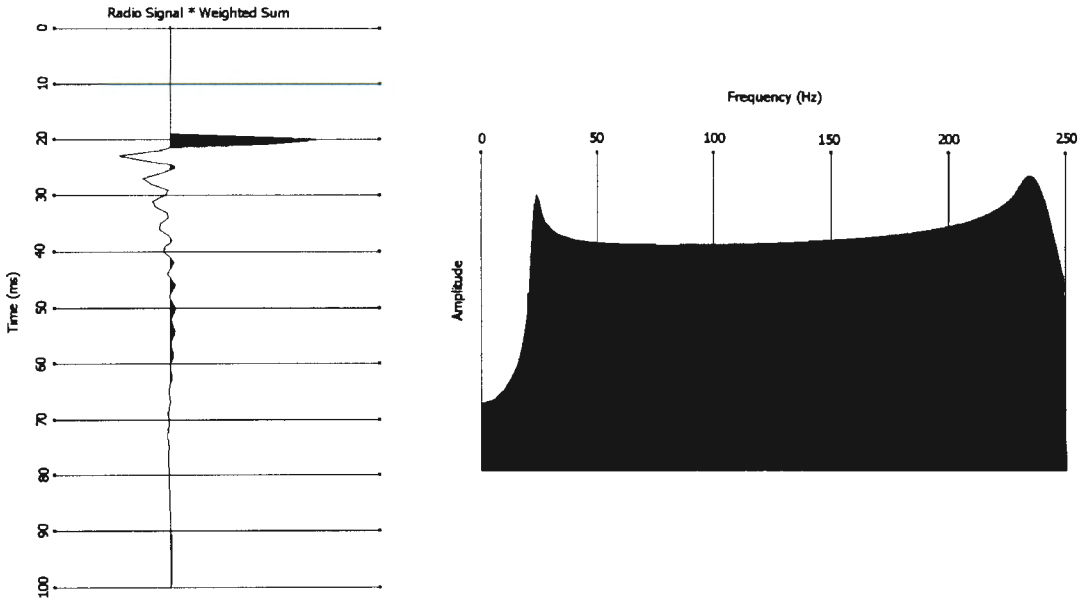


Figure 16. *(Left)* The wavelet is closer in appearance to a spike. *(Right)* Applying a time varying filter to the deconvolution eliminates noise in the radio.

Accelerometer Noise

Since the ground force is calculated using the signals generated by the motion of the baseplate and reaction mass, identifying accelerometer noise thresholds and reduction of that noise are crucial parts of this experiment. The IVI software on the Minivib's on board computer allows a lowest possible start frequency of 0.1 Hz, so background noise for the Dytran accelerometer was measured between 0.1 to 1.0 Hz, during a 10 s linear up-sweep. Noise in the frequency range 1 to 500 Hz was observed (recorded values < 1 Hz were ignored). As expected, the amplitude response from both accelerometers is very similar (Figure 17). The background noise for each accelerometer was compared to a typical recorded amplitude, for a 10 s, 10 – 500 Hz linear up-sweep (Figures 18 and 19). Values for dB, y, were calculated in Table 1 using the equation:

y = 20 log (sweep amplitude) – 20 log (background amplitude) (Serway and Beichner, 2000)

For example, at 105 Hz, the background noise at the baseplate is 45.6 dB down from the sweep. At the reaction mass, it is 27.9 dB down (see Table 1). Although the background noise is similar in amplitude, it is not surprising the amplitude of the measurement values between the locations for very different at the same frequency. This is because the amplitude spectra of the baseplate is different from the reaction mass.

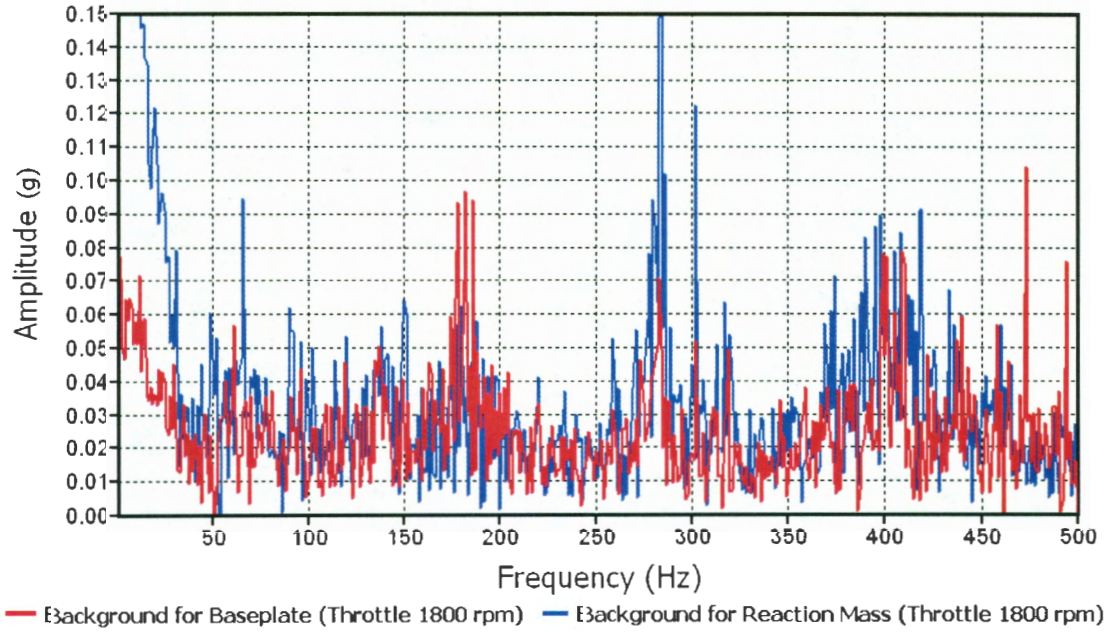


Figure 17. Background noise recorded at the baseplate and reaction mass. A low amplitude, 10 s linear up-sweep between 0.1 – 1.0 Hz was generated to record amplitudes up to 500 Hz. For this reason any values 1 Hz and below are omitted. The values are generally similar. The engine throttle is constant at 1800 rpm, which is a standard setting when acquiring data.

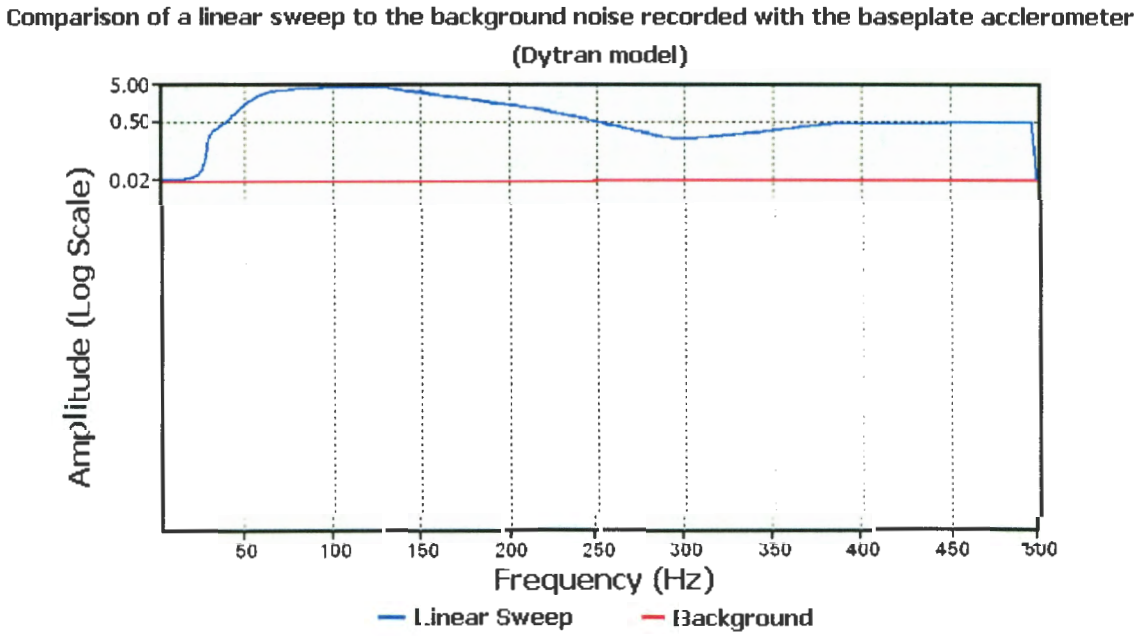


Figure 18. Graph showing the amplitude difference for the baseplate accelerometer between a typical sweep (blue) to recorded background noise (red) of the Dytran model.

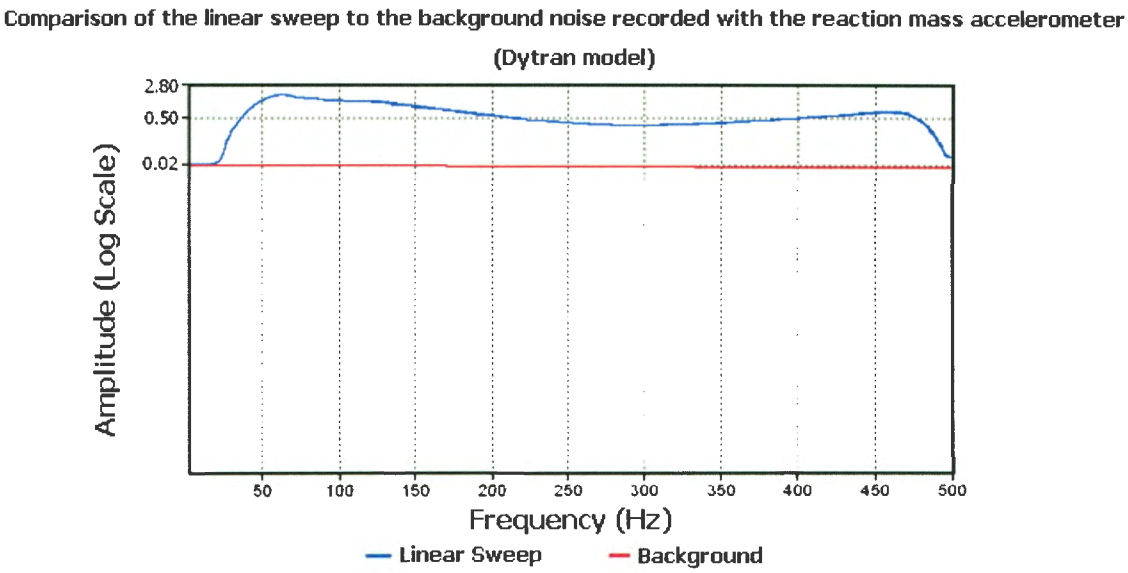


Figure 19. Graph showing the amplitude difference for the reaction mass accelerometer between a typical sweep (blue) to recorded background noise (red) of the Dytran model.

Baseplate (Dytran Model)			
Frequency (Hz)	**Sweep**	**Background**	**dB**
35	0.31	0.08	11.8
65	3.15	0.03	40.4
105	4.4	0.02	45.6
155	2.63	0.03	39.8
250	0.54	0.04	22.9
300	0.07	0.04	4.78
350	0.31	0.02	24.4
400	0.39	0.1	11.8
450	0.6	0.01	33.1

Reaction Mass (Dytran Model)			
Frequency (Hz)	**Sweep**	**Background**	**dB**
35	0.42	0.07	15.39
65	2.79	0.09	30.3
105	1.84	0.08	27.9
155	1.11	0.04	28.9
250	0.43	0.02	27.6
300	0.4	0.1	12
350	0.43	0.07	15.5
400	0.61	0.17	10.9
450	0.92	0.09	20.4

Table 1. Display of background and sweep amplitudes recorded at certain frequencies. Background amplitudes tend to be slightly higher for the reaction mass compared to the baseplate. Comparison of a 10-500 Hz sweep to the background noise determines the dB value. (Although the sweep values are different, the values in relation to the background are correct, hence, so is the dB value.)

For the Endevco model, the engine throttle was set to 1800 rpm for consistency with all the recording variables for the Dytran accelerometer. This measurement not only included the noise of the accelerometer amplifier, but the vibrator engine noise as well. Noise attributed to the engine will be discussed later. Figure 20 shows a visual relationship between the background noise and baseplate motion. Comparisions reveal the background noise is 59 dB down from the signal at 65 Hz (Table 2). Overall, the Endevco model yields an average noise threshold value that is 13 dB less than the Dytran model because it will on average,.

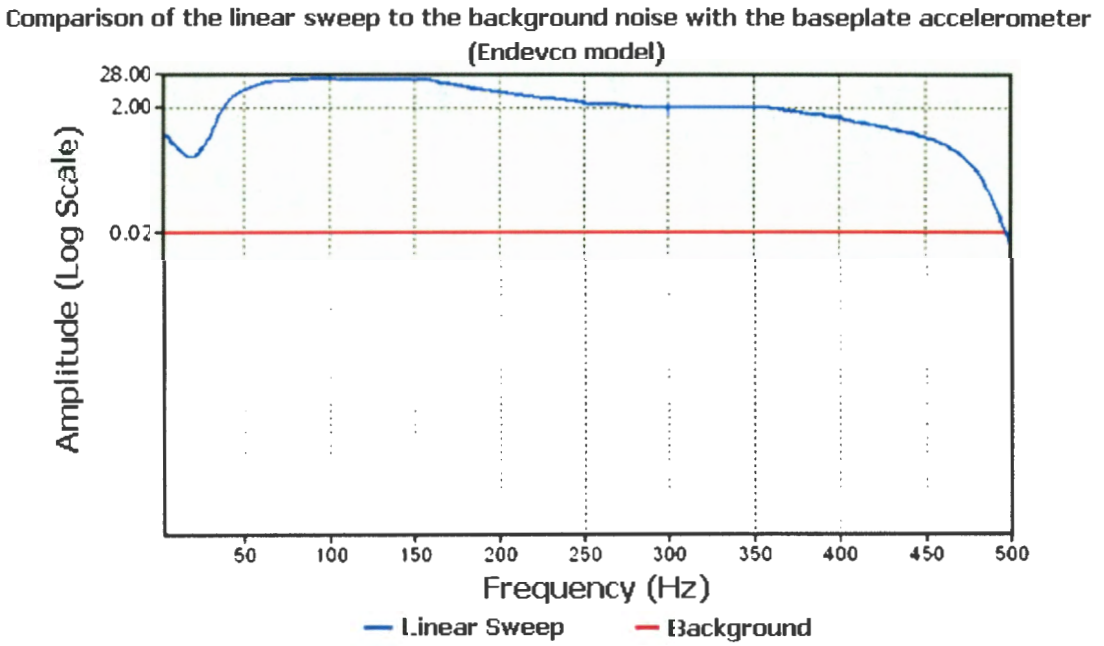


Figure 20. Graph showing the amplitude difference for the baseplate accelerometer between a typical sweep (blue) to recorded background noise (red) of the Endevco model.

Baseplate (Endevco Model)			
Frequency (Hz)	**Sweep**	**Background**	**dB**
35	1.31	0.033	32
65	17	0.019	59
105	20.3	0.073	48.9
155	17.1	0.047	51.2
250	3.75	0.023	44.2
300	2.17	0.036	35.6
350	2.16	0.081	28.5
400	2.89	0.107	28.6
450	0.47	0.031	23.5

Table 2. Display of background and sweep amplitudes recorded at certain frequencies for the Endevco model. Comparison of a 10-500 Hz sweep to the background noise determines the dB value.

IVI Minivib I Engine Noise

The Minivib's engine is another potential noise source that interferes with signal measured by the accelerometers. It was mentioned earlier that due to software limitations the Dytran accelerometers are unable to be used without the engine running. In addition, the throttle must be set to a least 1500 rpm for uniform mechanical and fluid performance, which is why all measurements were taken a 1800 rpm, similar to field conditions.

The Endevco accelerometer was used for quantifying the amount of engine noise recorded through the baseplate accelerometer. This was done by recording the background noise twice: once with the engine off, and then with the engine on.

Variations between the two frequency spectra confirmes engine noise is present (Figure 21). Table 3 reveals that a significant percentage of noise recorded by the accelerometer on the baseplate can be attributed to engine noise. For example, at 105 Hz, 92.1% of noise recorded by the accelerometer can be accredited to engine noise, and the remaining 7.9% is accelerometer amplifier noise. Overall, the average percentage between 1 to 499 Hz is 71.9%. Figure 22 shows the noise produced from the engine as recorded on the frame. The amplitude is on the order of 10^3 times higher than what is recorded on the baseplate. The average percentage of engine noise recorded by the baseplate accelerometer is only 0.02% of the total vibration produced. Since this value is so low, the baseplate can be considered vibrationally isolated from the engine.

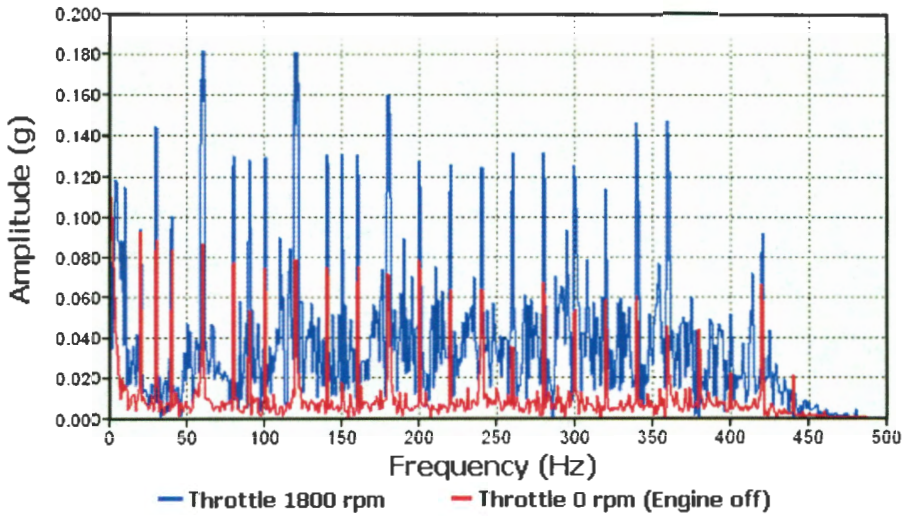


Figure 21. Background noise was recorded with the Minivib engine set to 1800 rpm *(blue)* and with the engine off *(red)*.

Endevco 7703A-1000			
Frequency (Hz)	Throttle 1800 rpm	Throttle 0 rpm (Engine off)	%
35	0.033	0.004	86.7
65	0.019	0.009	55.2
105	0.073	0.006	92.1
155	0.047	0.006	87.5
250	0.023	0.014	40.2
300	0.036	0.011	68.7
350	0.081	0.011	85.9
400	0.107	0.032	70.6
450	0.031	0.006	80.5

Table 3. Comparison of accelerometer measurements with the engine throttle set to 1800 rpm and with the engine off. It is revealed that for most frequencies the majority of noise is due to engine noise.

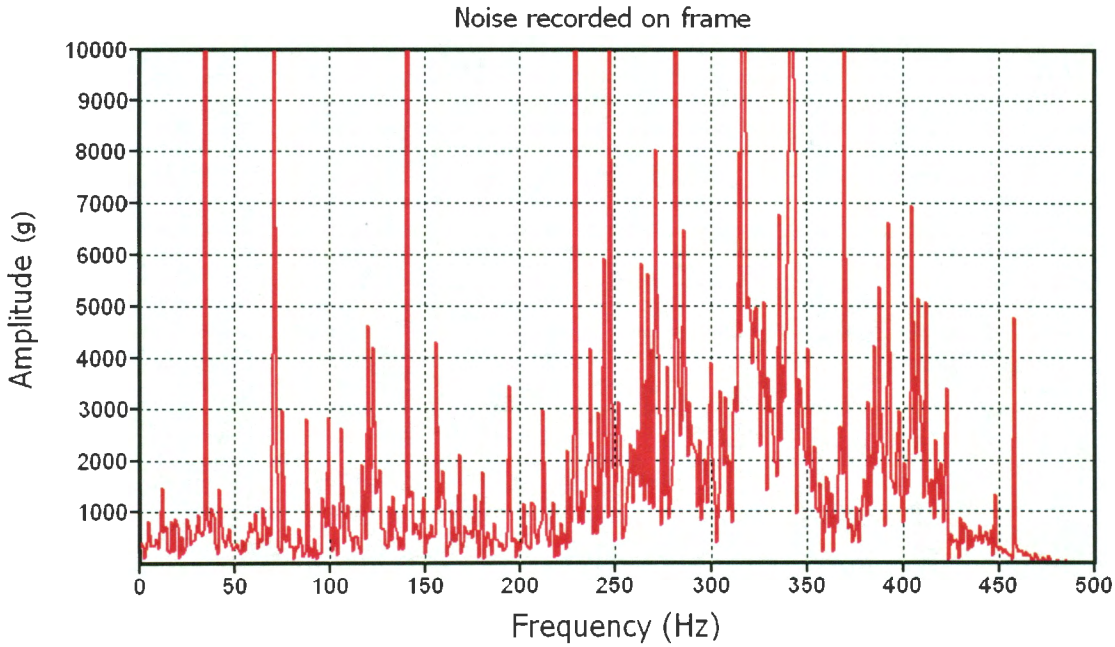


Figure 22. Noise generated from the engine as recorded on the frame.

Summary for Pre-survey Provisions

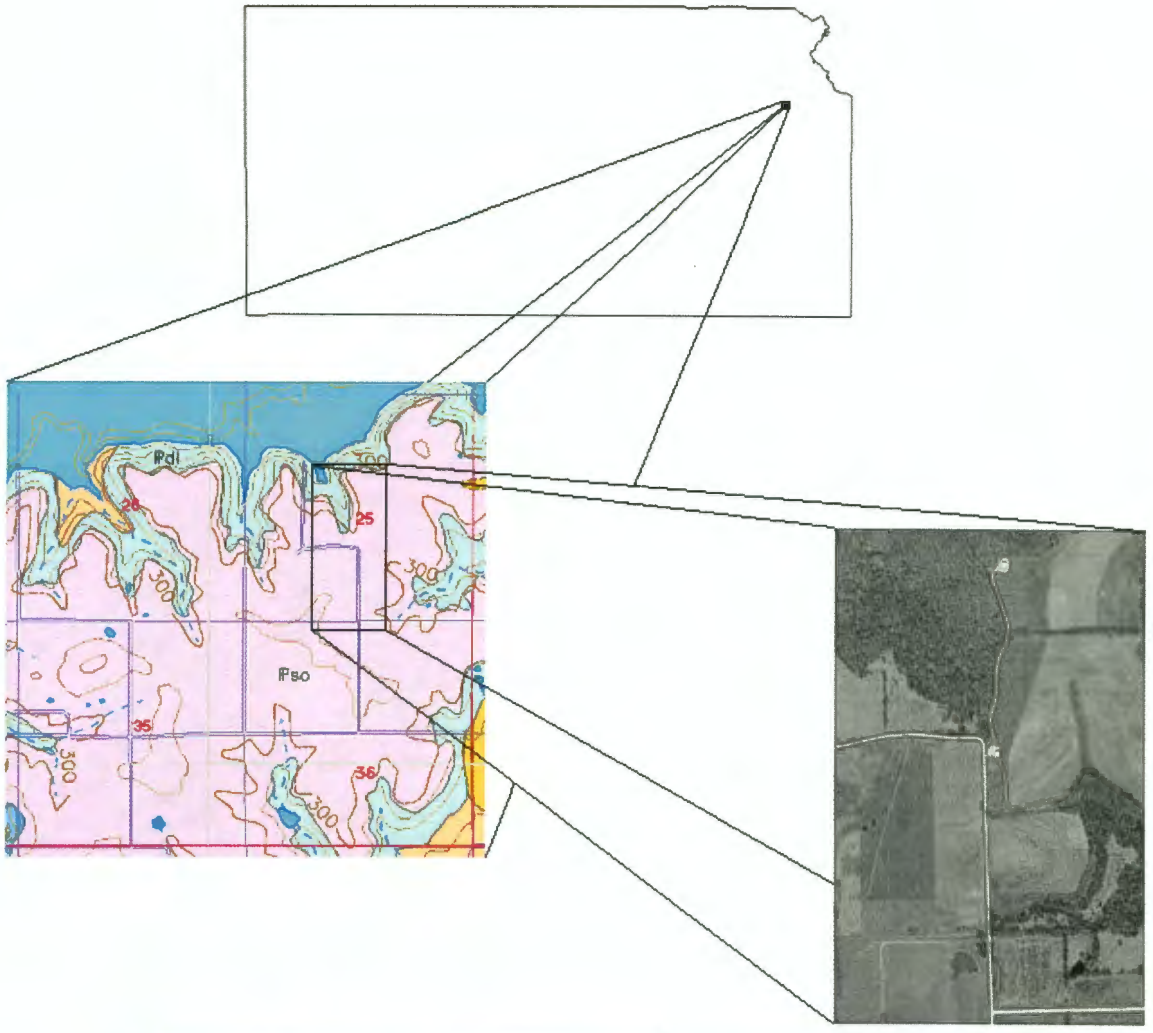
Noise within telemetry system and accelerometers can be reduced. The telemetry system noise can be attenuated by applying a time varying filter. By using the Endevco accelerometer over the Dytran model noise can be reduced by an average of 13 dB. Moreover, the engine is responsible for about 72% of the noise recorded by the Endevco accelerometer on the baseplate, however, this is only 0.02% of vibration that is recorded during a typical sweep. For this reason, it can be assumed that the baseplate is vibrationally isolated from the Minvib's engine.

Adams Campus Survey

Achieving optimized high-frequency vibroseis data is done by deconvolving the recorded seismic energy with the ground force, which requires accurate measuring of the true ground force (Bickel, 1982). The measurements recorded by the accelerometers must be equivalent to the ground force that is actually propagating through the ground. Deviation from the true ground force so far has been attributed to accelerometer electrical noise, engine noise picked up by the baseplate accelerometer, and radio signal distortion. The rest of this study focuses on the position of the baseplate accelerometer and changes due to flexure, phase and amplitude changes.

Geology

Experiments were conducted on Adams Campus in Douglas County, KS where surficial geology is dominated by Pennsylvanian age units (Figure 23). A dry and abandoned oil well located 10 miles east of Adams Campus depicts the lithology of the region (Figure 24). The subsurface rocks in the area consist of Pennsylvanian cyclic limestone and shale sequences with a total thickness of 270 m, overlying a 75 to 120 m thick uniform Mississippian limestone layer (Ball et al., 1963). The location of the limestone and shale beds are evident on gamma ray and neutron porosity readings from the well (Figure 25). The physical characteristics of these limestone layers make this site an ideal conducting tests of this type because seismic velocity will be high and attenuation relatively low (Levin, 1979), however near surface soil conditions can make velocity interpretation problematic because velocity tends to be low in the first several meters (Vossen et al., 2005), which is the target depth.



Quaternary
Pleistocene Series

- Qal Alluvium
- Qtn Newman Terrace deposits
- Qtbc Buck Creek Terrace deposits
- Qtu Undifferentiated terrace and colluvial deposits
- Qkt Qko Till and upland glacio-fluvial deposits

Pennsylvanian
Virgilian Series
Shawnee Group

- Pst Topeka Limestone
- Psdc Calhoun Shale and Deer Creek Limestone
- Pstl Tecumseh Shale and Lecompton Limestone
- Pso Kanwaka Shale and Oread Limestone

Douglas Group

- Pdl Lawrence Formation
- Pds Top of Haskell Limestone to the base of Tonganoxie Sandstone of Stranger Formation
- Ppw Base of Tonganoxie Sandstone (Stranger Formation) to the top of Stanton Limestone

Missourian Series
Lansing Group

- Pls Stanton Limestone
- Plv Vilas Shale and Plattsburg Limestone

Figure 23. Location and aerial photo of Adams Campus depicts the local geology, which consists of Pennsylvanian limestone and shale.



Figure 24. Location of Adams Campus and well Boehle 7 in Douglas County.

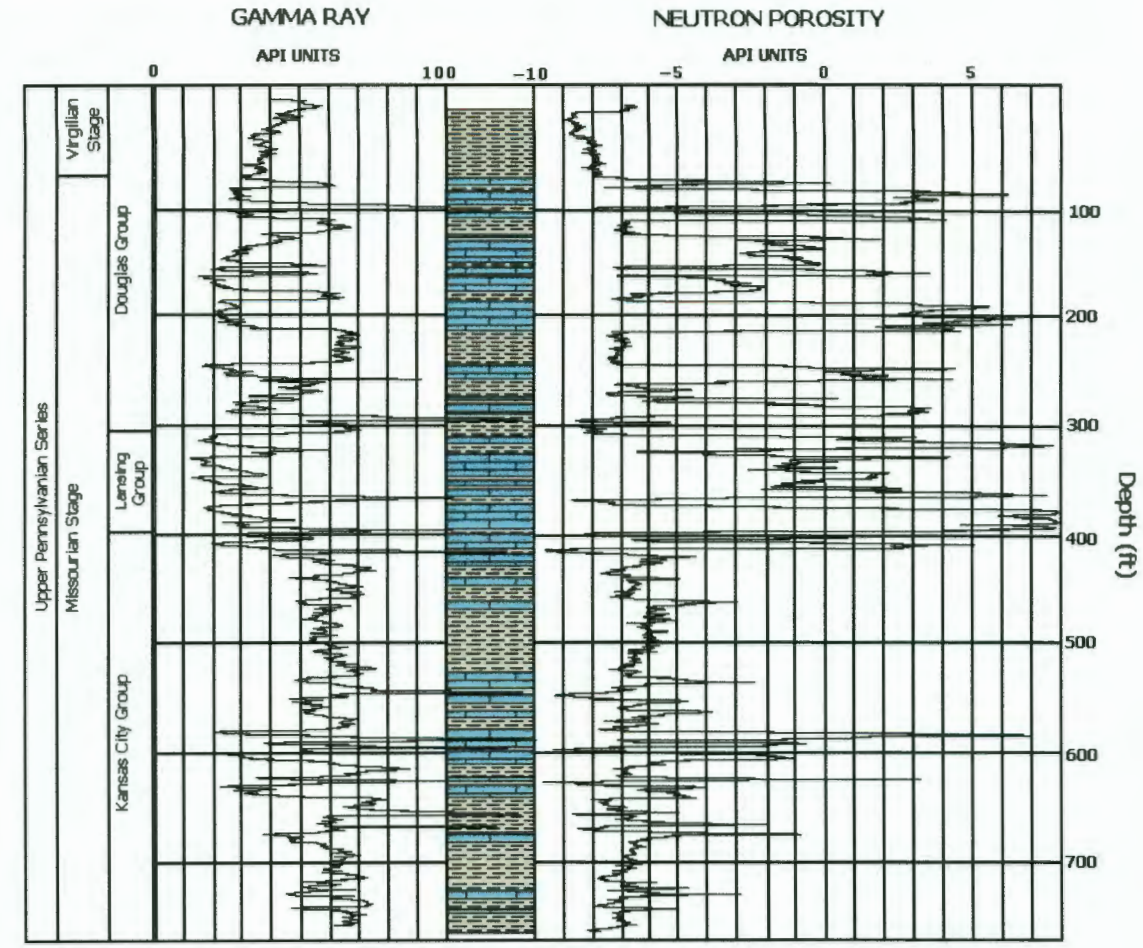


Figure 25. Gamma ray and neutron porosity log taken from a borehole located in Douglas County. The lithology in the area consists of limestone and shale, which is consistent with the upper Pennsylvanian Series.

Equipment and Acquisition Methods

Understanding vibrator-earth interaction is an important aspect for optimizing transmission of high frequencies (Seriff and Kim, 1970; Schrodt, 1985; Schrodt et al, 1987). Baseplate coupling with the ground will change depending on the surface type, such as sand, cement, and full or partial contact. Amplitude and phase control of vibrator output is significantly more difficult on rigid ground. To prove that high frequencies can be optimized for any given soil variation, the proof must be true for the worst-care scenario because it is the most convincing.

Baseplate flexure is another issue for concern. Brook and Crews (1991) did experiments on circular baseplates revealing up to a 20 degree phase shift from what was being measured between 32 different baseplate accelerometer locations. This study attempts to do something similar to Brook and Crews experiment by choosing different locations for the accelerometer and comparing them to velocity measurements recorded by a buried geophone. HFVS makes the assumption that the derivative of the ground force is in phase with velocity measurements however, Allen et al. (1998) goes on to discuss a 60 degree phase shift at 140 Hz. Preliminary testing was done on accelerometer data and 90 degree shifted velocity data to determine if comparing accelerometer data to velocity data would be problematic. Testing revealed that phase shifted velocity data still correlated to 80% of the original accelerometer data, with 20% attributed to waveform differences. For these reasons, the assumption is made that the ground force can be compared to velocity data.

Two 28 Hz geophones were planted below 2 ft of ground in cement (Figure 26). The Minivib's baseplate was placed over these geophones for the duration of the study

(Figure 27). The assumption here is that during a sweep, these geophones would record the true signal transmitted into the ground. This signal could then be compared to the ground force calculated using the reaction mass and baseplate accelerometers similarity would be a measure of optimal instrumentation of vibrator. Five positions on the baseplate were decided upon for locating the Endevco baseplate accelerometer (Figure 28).

The survey was set up in a north/south orientation (Figure 29). A line of receivers consisting of thirty twin 40 Hz Mark products L28E geophones separated by 1.22 m (Figure 30). The data acquired by theses geophones were used to determine attenuation due to spherical divergence and absorption.

Two sweep types were used for these tests: 1) a 10 s, linear up-sweep from 20–500 Hz, with a front taper of 0.25 s and end taper of 0.1 s, and 2) a 5 sec, linear up-sweep from 200-500 Hz with a front taper of 0.25 s and end taper of 0.1 s. During the study, the Endevco accelerometer was systematically placed in each of the five predetermined locations. Drive amplitudes, controlling how much force is applied to the mass, were varied to avoid receiver clipping that would not corrupt the data. For the 20-500 Hz, the reference drive amplitude was maintained at the systems minimum to avoid overdriving receivers due to the lower attenuation of lower frequencies. Since the annenuation is significant at higher frequencies, the reference drive amplitude was increased by 5 times for the 200-500 Hz sweeps.



Figure 26. The two 28 Hz geophones are buried underneath cement while their connectors allow seismic information to be recorded via the takeout cables.

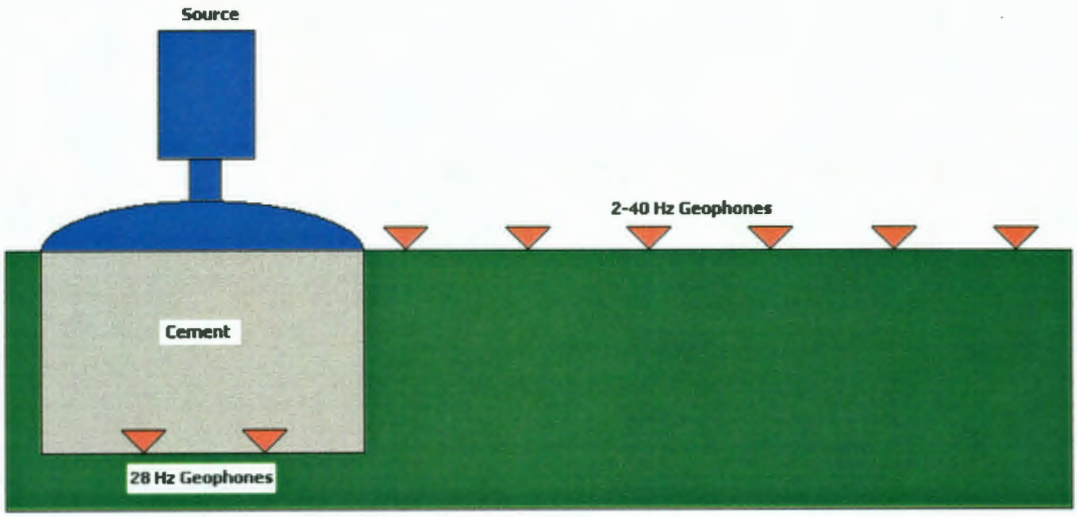
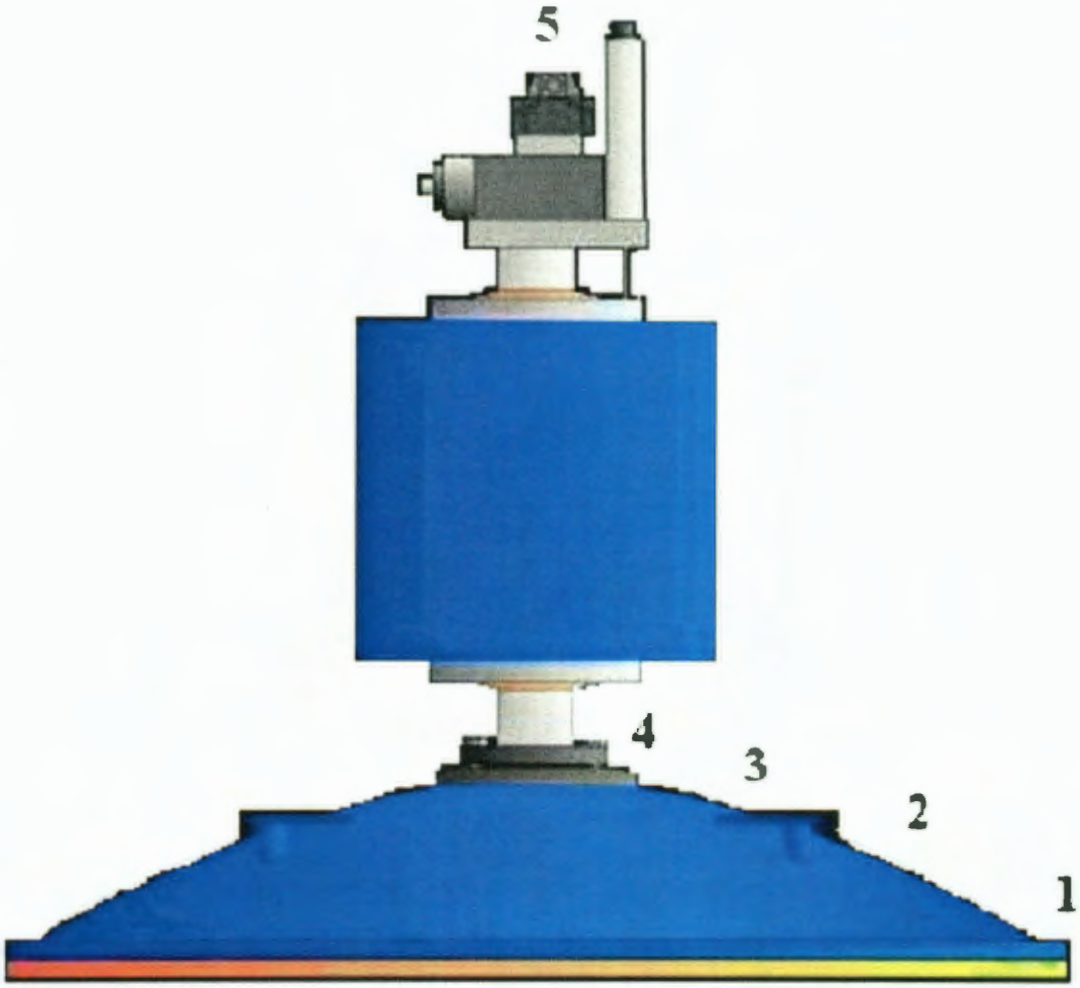


Figure 27. Schematic of the survey setup.



Endevco accelerometer location	Distance from center
Position 1	18"
Position 2	14.25"
Position 3	10.5"
Position 4	6.5"
Position 5	0"

Figure 28. The five locations of the Endevco accelerometer.



Figure 29. Location of the survey on Adams Campus. The geophone array consisted of 2-40 Hz geophones with 4 ft spacing.



Figure 30. Photo of a 2-40 Hz geophone connected to a black takeout cable.

Processing and Results

Determining ground response and identifying the best source instrumentation was done by comparing the possible ground force measurements. Source measurement based on the ground force that best resembles ground response is the first objective. The second objective is to determine optimal frequency ranges of signal. Due to the aforementioned anti-aliasing filter in the NZC seismograph, correlation of ground response with source measurement was broken up into two main parts. The first is a frequency range of 20-250Hz. The second frequency range is 200-500 Hz.

0-255 Hz

Although the focus of this experiment is on high frequency spectra, the low frequency range was also examined because many surveys done by the KGS are confined to this frequency range. A band-pass filter (0-20-240-255) was applied to the accelerometers and geophones that recorded a 20-500 Hz, 10 s linear upsweep to observe only lower frequencies (Figure 31). Correlation of the 28 Hz geophone response with the baseplate and reaction mass measurements reveals that the configuration that is most similar to the 28 Hz geophone(s) is the Endevco accelerometer located on the baseplate (Figure 32). This accelerometer is similar, on average, to 87% of the ground measurement in the frequency bandwidth, however, this value will fluctuate depending on its location on the baseplate. Figure 33 shows that with further analysis, position 3 is the best location for the accelerometer providing a correlation of 89.46%.

The error bars were determined using the standard deviation. The most significant overlap is with the ground force and baseplate accelerometer meaning that the reaction mass accelerometer cause no change in correlation (Endevco). Furthermore, Figure 33 shows that the ground force calculation and baseplate accelerometer measurement are the same value within the measurement precision.

While correlation numerically states which one is most similar, deconvolution visually validates it (Figure 34). The three configurations that are most like the 28 Hz geophone are recorded with the Endevco model, which are the reaction mass acceleration, baseplate acceleration and the ground force. Figure 35 further reveals the result of deconvolution in the frequency domain. This confirms that the measurements

recorded with the Endevco model are most similar to the 28 Hz geophone, and moreover, position 3 is the best location for the accelerometer.

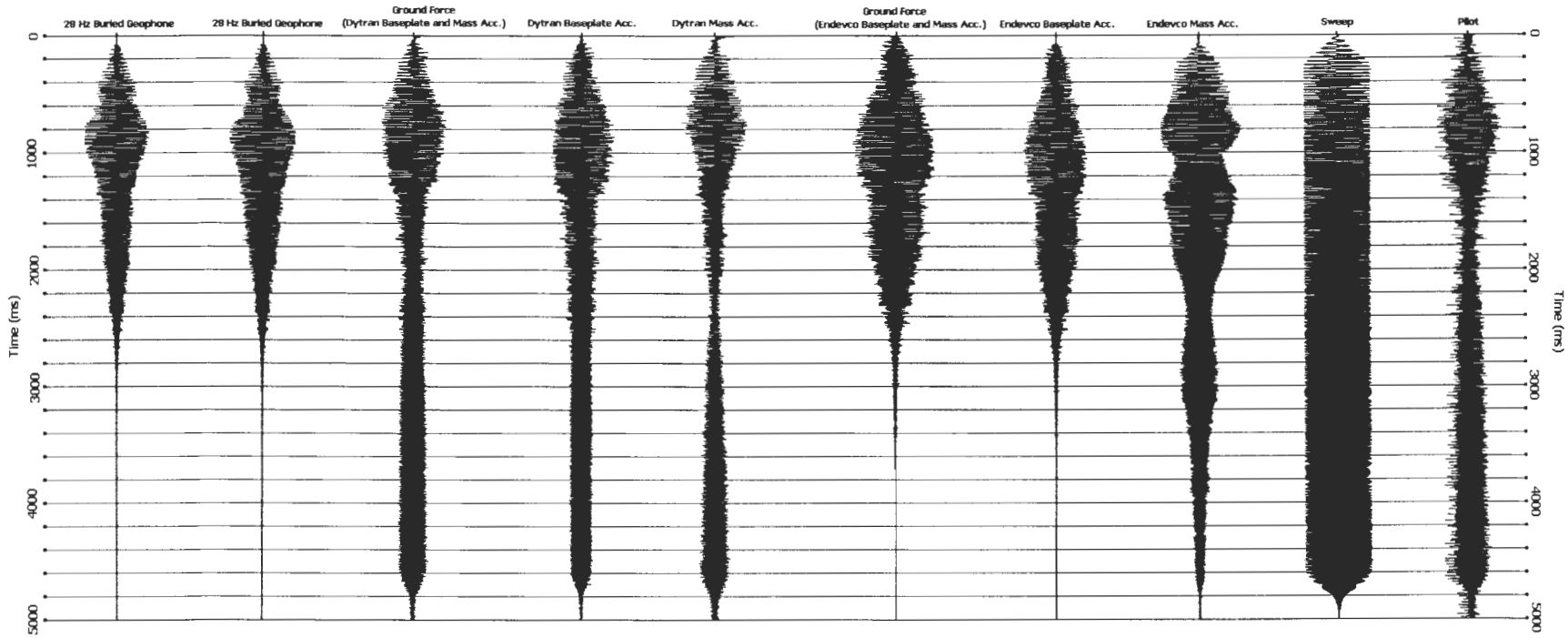
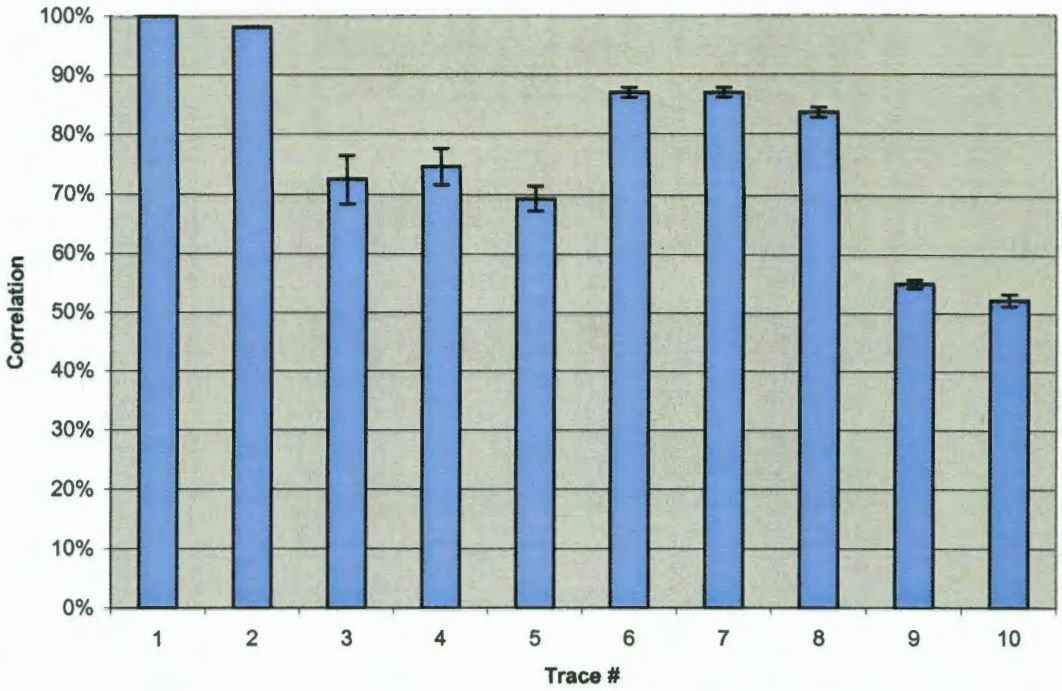
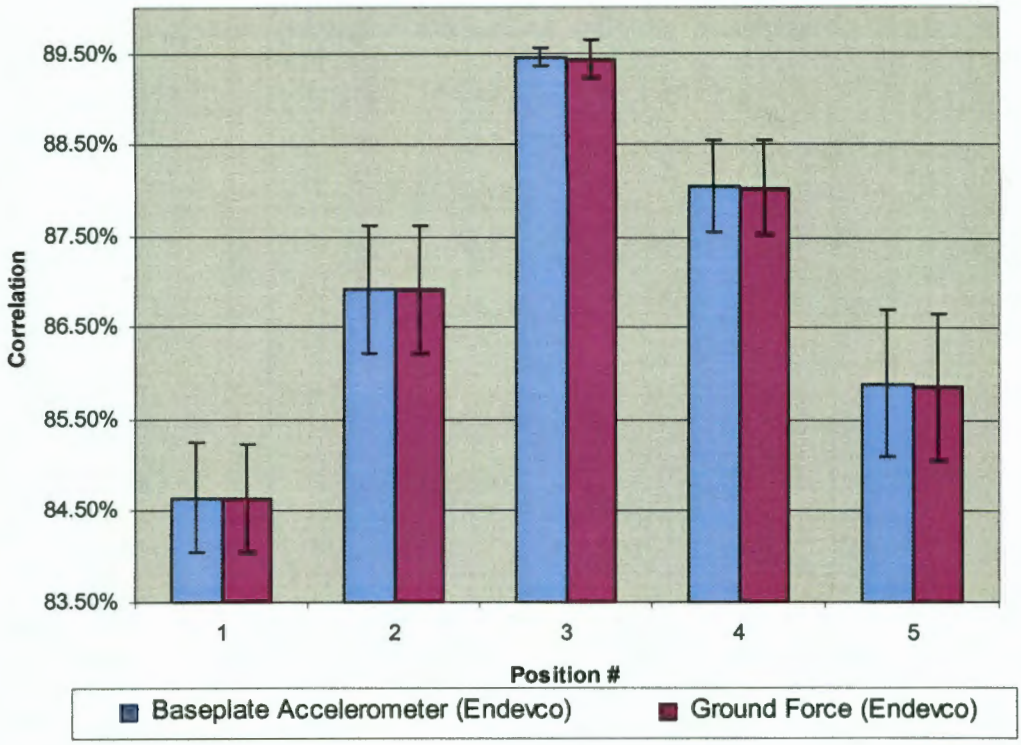


Figure 31. Various geophone and accelerometer responses and synthetic sweep to a 10 sec. linear up-sweep with a low frequency (0-20-240-255) bandpass filter.



Trace #	Correlation with Trace 1
1: 28 Hz Buried Geophone	100%
2: 28 Hz Buried Geophone	98.10%
3: Weighted Sum (Dytran Baseplate and Mass Acc.)	72.43%
4: Dytran Baseplate Acc.	74.57%
5: Dytran Mass Acc.	69.35%
6: Weighted Sum (Endevco Baseplate and Mass Acc.)	86.98%
7: Endevco Baseplate Acc.	87.00%
8: Endevco Mass Acc.	84%
9: Sweep	55.02%
10: Pilot	52.30%

Figure 32. Correlation with the 28 Hz phone reveals that the Endevco accelerometer on the baseplate yields the highest fidelity of ground response.



Trace #	Positions of the Endevco Model on the Baseplate				
	Position 1 (18" from center)	Position 2 (14.25")	Position 3 (10.5")	Position 4 (6.5")	Position 5 (0")
6: Weighted Sum (Endevco Baseplate and Mass Acc.)	84.64%	86.92%	89.44%	88.05%	85.87%
7: Endevco Baseplate Acc.	84.65%	86.93%	89.46%	88.06%	85.90%

Figure 33. Correlation with the 28 Hz geophone and the Endevco accelerometer located on the baseplate reveals that placement makes a difference in signal response. Position 3 yields the best response with the least amount of error in measurement.

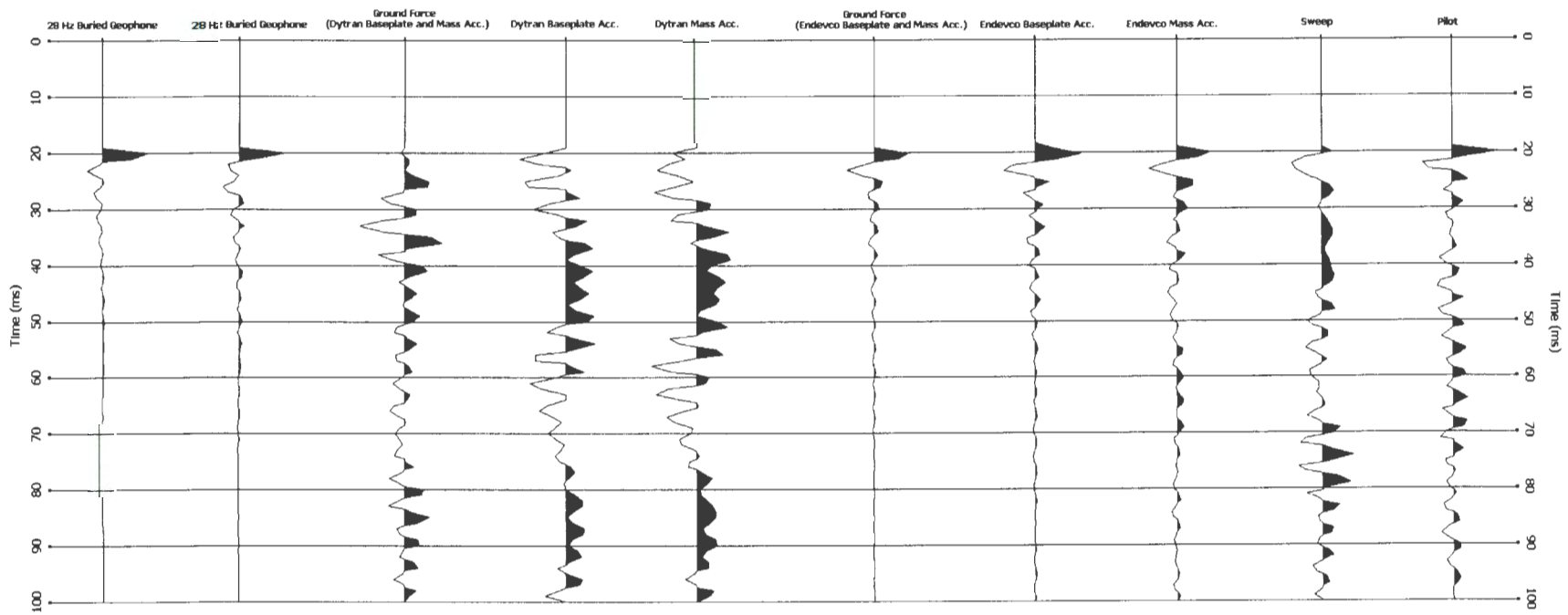


Figure 34. Deconvolution with the 28 Hz buried geophone. This visually supports how the waveform of the Endeveo baseplate accelerometer is the best measurement of the true ground force.

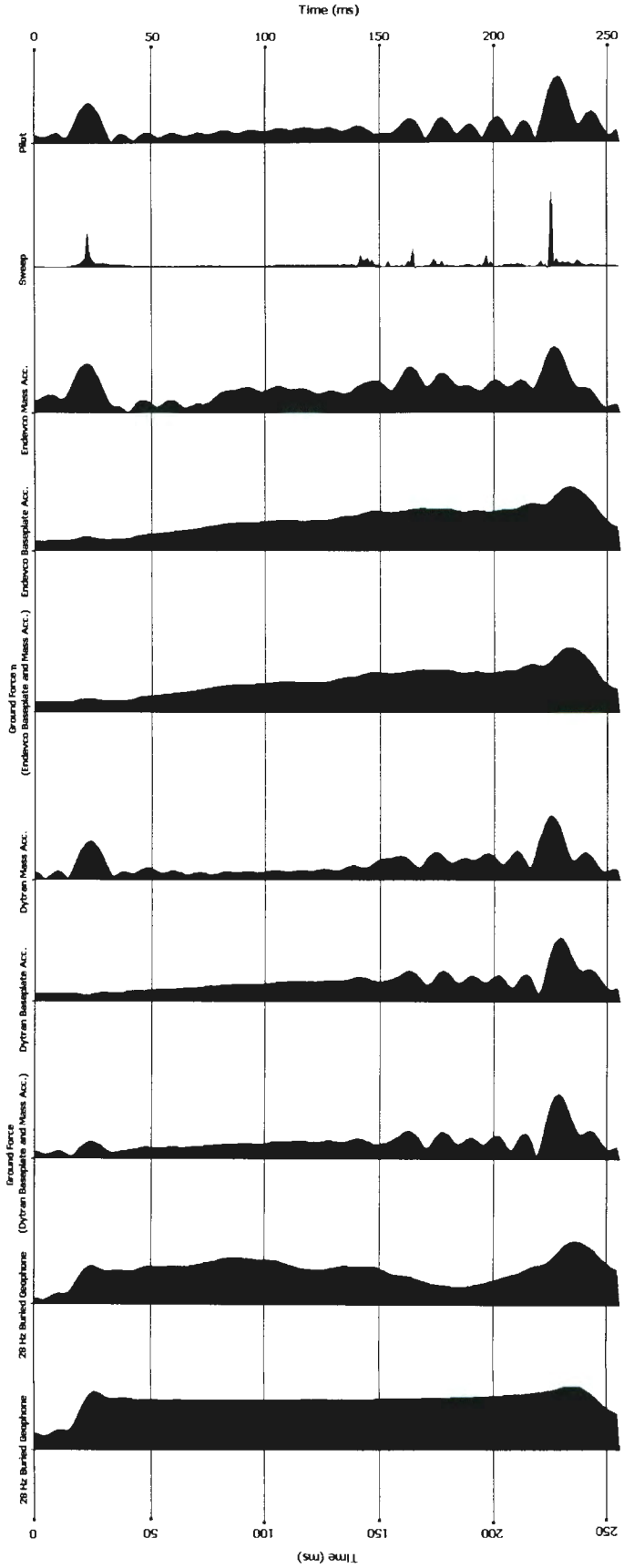


Figure 35. The frequency spectrum after deconvolution.

200-500 Hz

A second experiment was undertaken to determine the best location of the baseplate accelerometer for high frequencies only. The source produced a 5 sec, 200-500 Hz linear up-sweep (Figure 36). For this survey, only one 28 Hz geophone was working in the cement post. Correlation with the 28 Hz geophone reveals that the Endevco mass accelerometer is a configuration that chacterizes signal if the various baseplate positions are averaged with a value of 83.79% (Figure 37). Further analysis reveals that the Endevco baseplate accelerometer response is highly dependent on location, and moreover, yields the highest similarity with the 28 Hz geophone. Position 2 is the location that one would want to use for this particular frequency range because it correlates to 87.4% of the true signal (Figure 38). Positions 3 and 4 are very close in value to position 2. Moreover, position 2 yields a better reading than the ground force calculated using position 2, which has an average value of 84% ± 2%. Figures 39 and 40 further reveal the result of deconvolution in the frequency domain. This confirms the Endevco configurations yield the most accurate measurements.

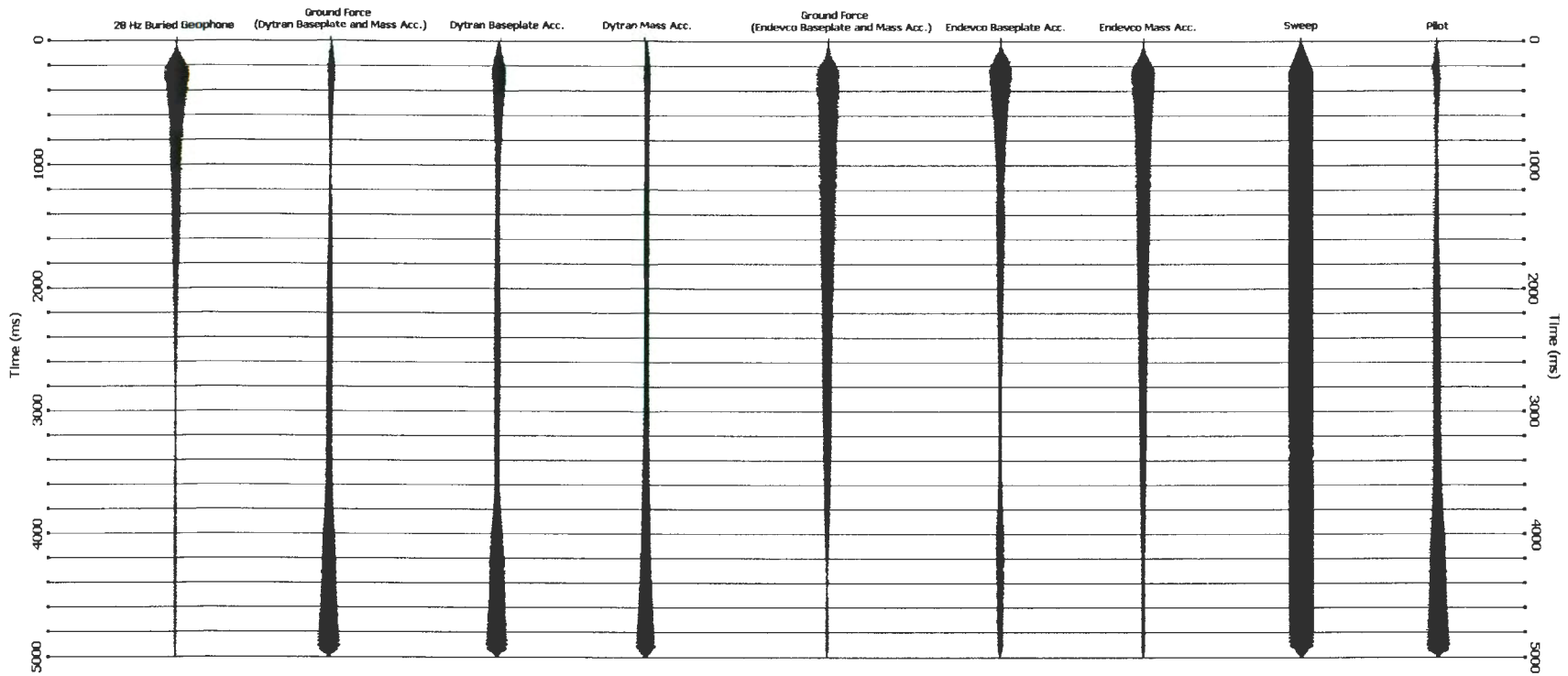
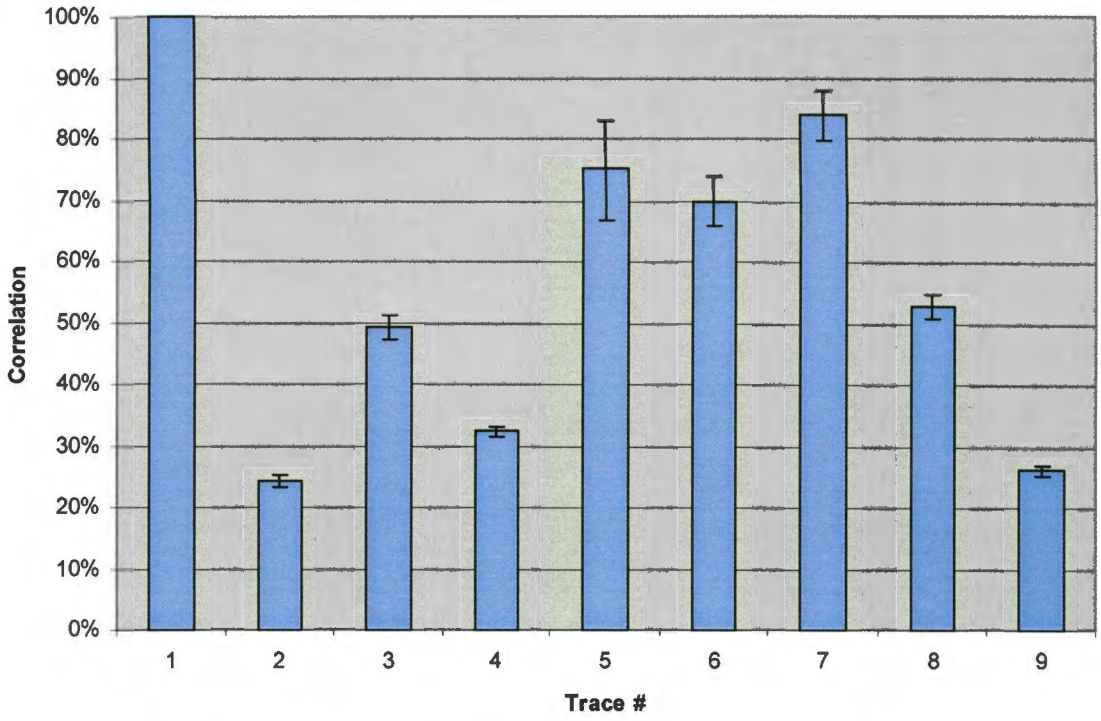
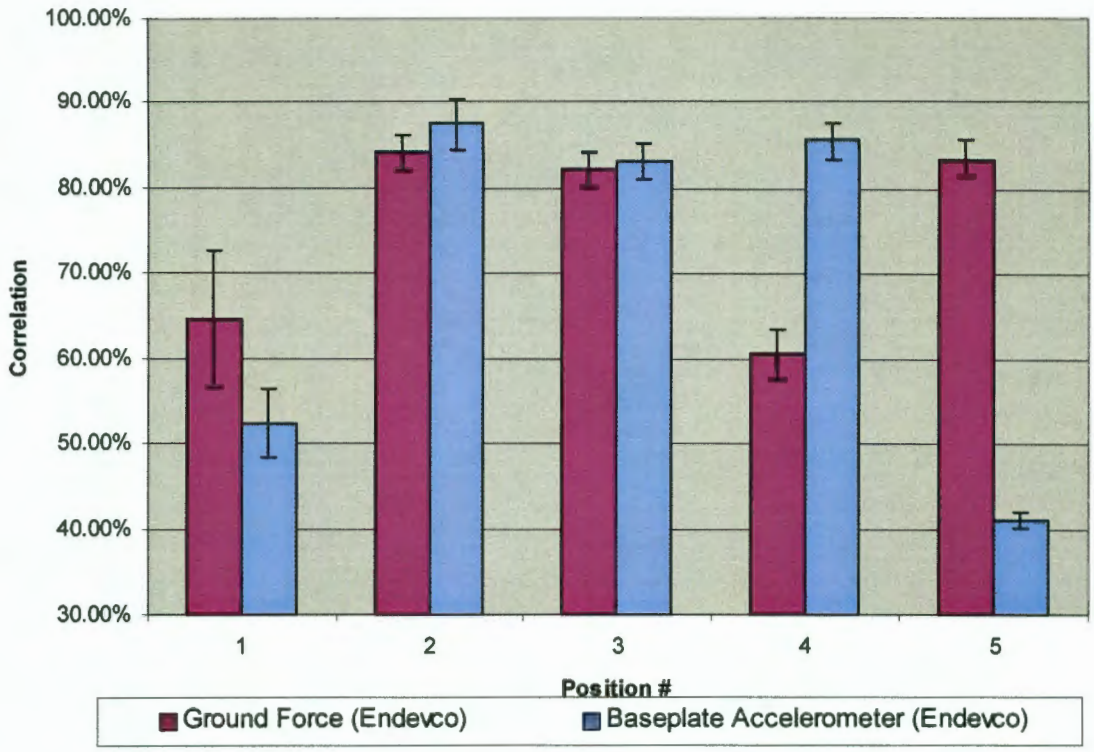


Figure 36. Various geophone and accelerometer responses and synthetic sweep to a 5 sec, linear up-sweep with a high frequency range of 200-500 Hz.



Trace #	Correlation with Trace 1
1: 28 Hz Buried Geophone	100%
2: Ground Force (Dytran Baseplate and Mass Acc.)	24.24%
3: Dytran Baseplate Acc.	49.20%
4: Dytran Mass Acc.	32.37%
5: Ground Force (Endevco Baseplate and Mass Acc.)	75.03%
6: Endevco Baseplate Acc.	69.93%
7: Endevco Mass Acc.	83.79%
8: Sweep	52.79%
9: Pilot	26.08%

Figure 37. Correlation with the 28 Hz phone reveals that the Endevco mass accelerometer yields the highest fidelity of ground response when position is not accounted for on the baseplate.



Trace #	Positions of the Endevco Model on the Baseplate				
	Position 1 (18" from center)	Position 2 (14.25")	Position 3 (10.5")	Position 4 (6.5")	Position 5 (0")
5: Ground Force (Endevco Baseplate and Mass Acc.)	64.66%	84.10%	82.29%	60.58%	83.52%
6: Endevco Baseplate Acc.	52.47%	87.40%	83.18%	85.54%	41.04%

Figure 38. Correlation with the 28 Hz geophone and the Endevco accelerometer located on the baseplate reveals that placement makes a difference in signal response. Position 2 yields the best response, beating out the mass accelerometer and the ground force.

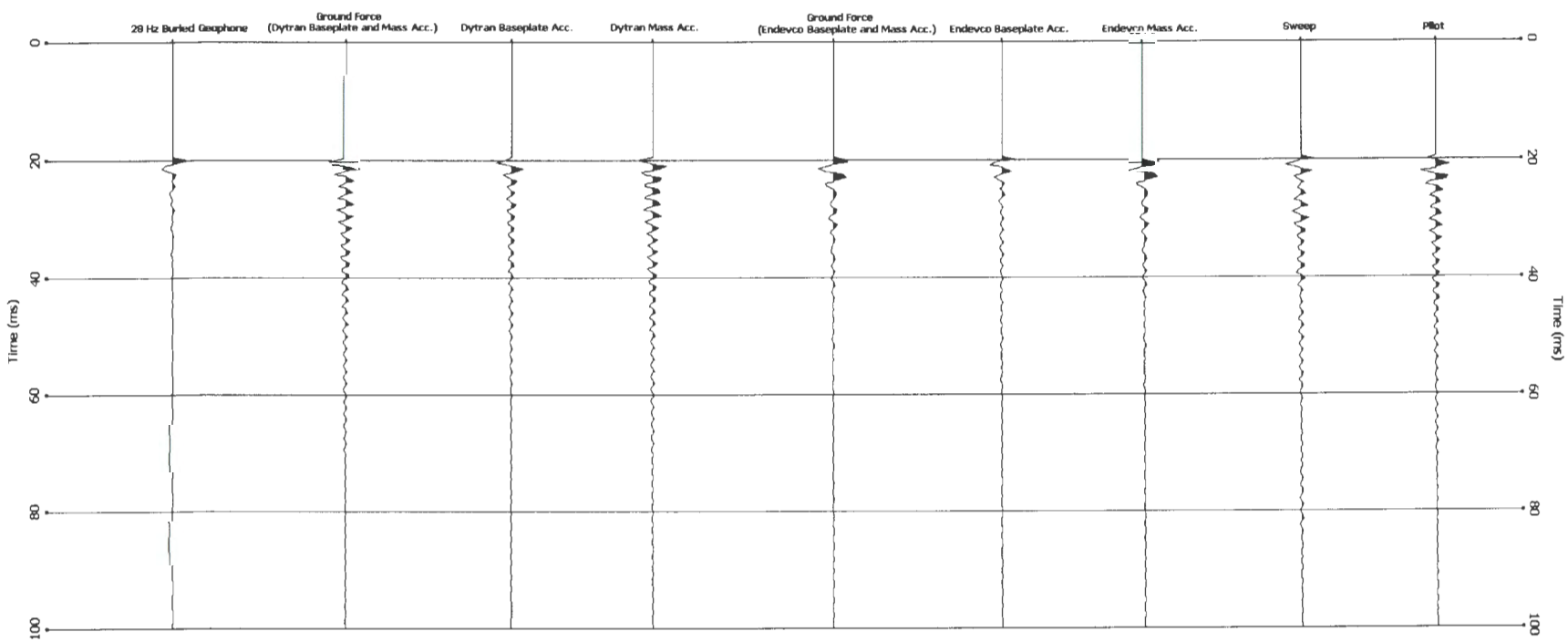


Figure 39. Deconvolution with the 28 Hz buried geophone for a linear upsweep with a frequency range 200-500 Hz. This visually supports how the waveform of the Endevco baseplate accelerometer is the best measurement of the true ground force.

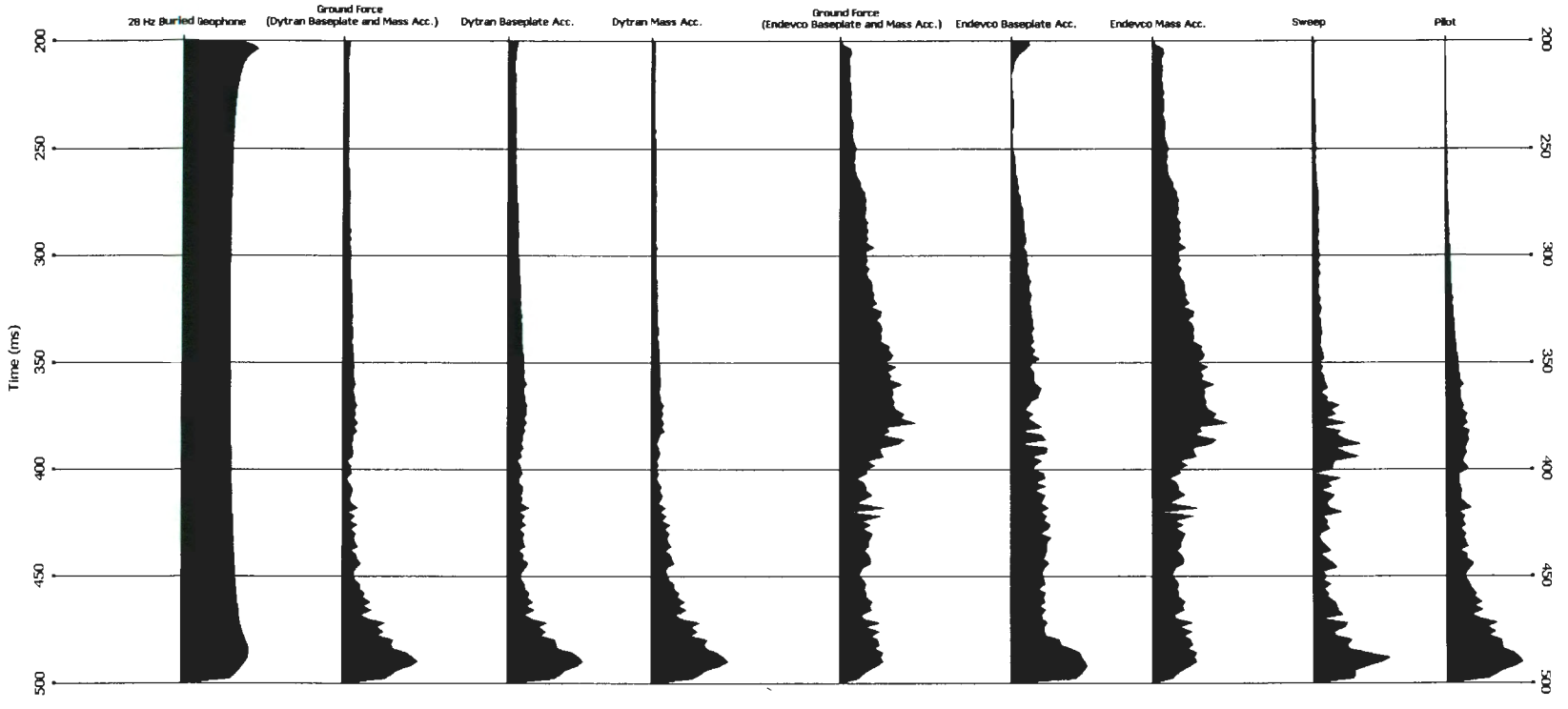
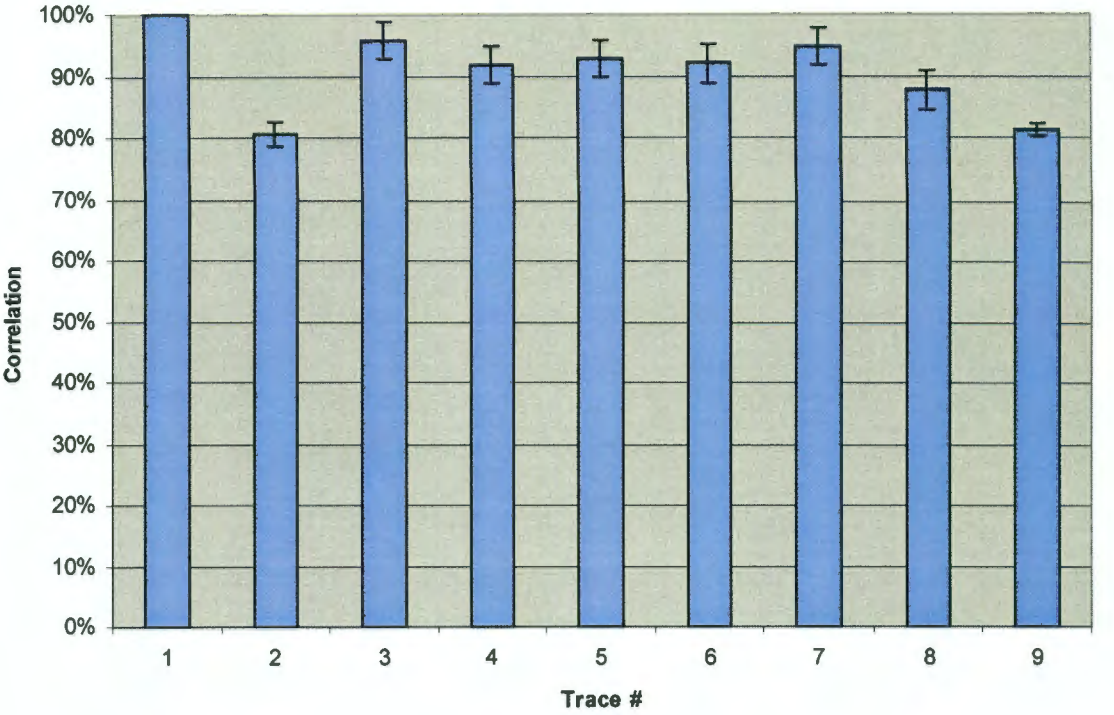


Figure 40. Deconvolution with the 28 Hz buried geophone for a frequency range of 200-500 Hz. This visually supports how the waveform of the Endevco baseplate accelerometer is the best measurement of the true ground force.

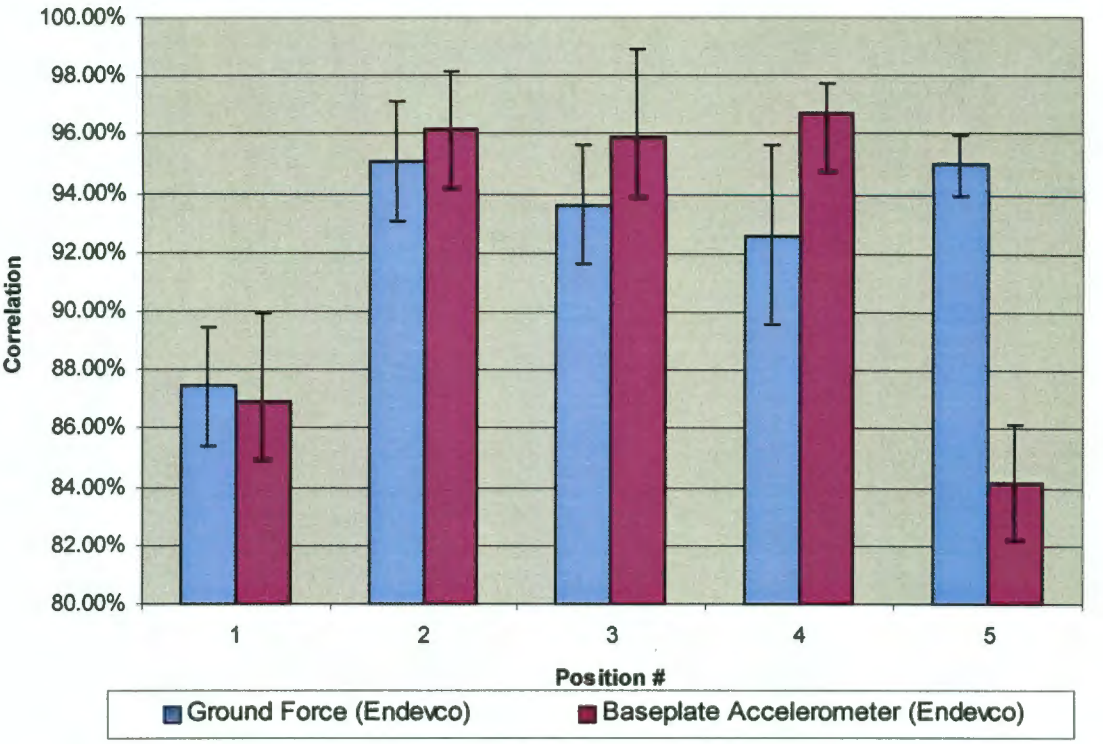
200-300 Hz

By breaking the data set into three frequency bands, it is possible to delineate specific ranges of optimized measurements. This is important because it can identify frequency ranges that may be more susceptible to harmonics or resonance. A band pass filter (200-220-300-320) was applied to the 28 Hz geophone and the accelerometer measurements to determine the correlation coefficients with the 28 Hz geophone (Figure 41) and again, the Endevco baseplate accelerometer provides a response most similar to the 28 Hz geophone placed at position 4 (96.73% ± 1%) (Figure 42). Moreover, position 2 (96.18% ± 3%) and position 3 (95.92% ± 2%) are very close in value to position 4. It should be noted that there is a significant drop-off in signal measurement at the rim and center of the baseplate.



Trace #	Correlation with Trace 1
1: 28 Hz Buried Geophone	100%
2: Ground Force (Dytran Baseplate and Mass Acc.)	80.63%
3: Dytran Baseplate Acc.	95.64%
4: Dytran Mass Acc.	91.73%
5: Ground Force (Endevco Baseplate and Mass Acc.)	92.75%
6: Endevco Baseplate Acc.	91.99%
7: Endevco Mass Acc.	94.68%
8: Sweep	87.74%
9: Pilot	81.37%

Figure 41. Correlation with the 28 Hz phone reveals that the Endevco mass accelerometer yields the highest fidelity of ground response.

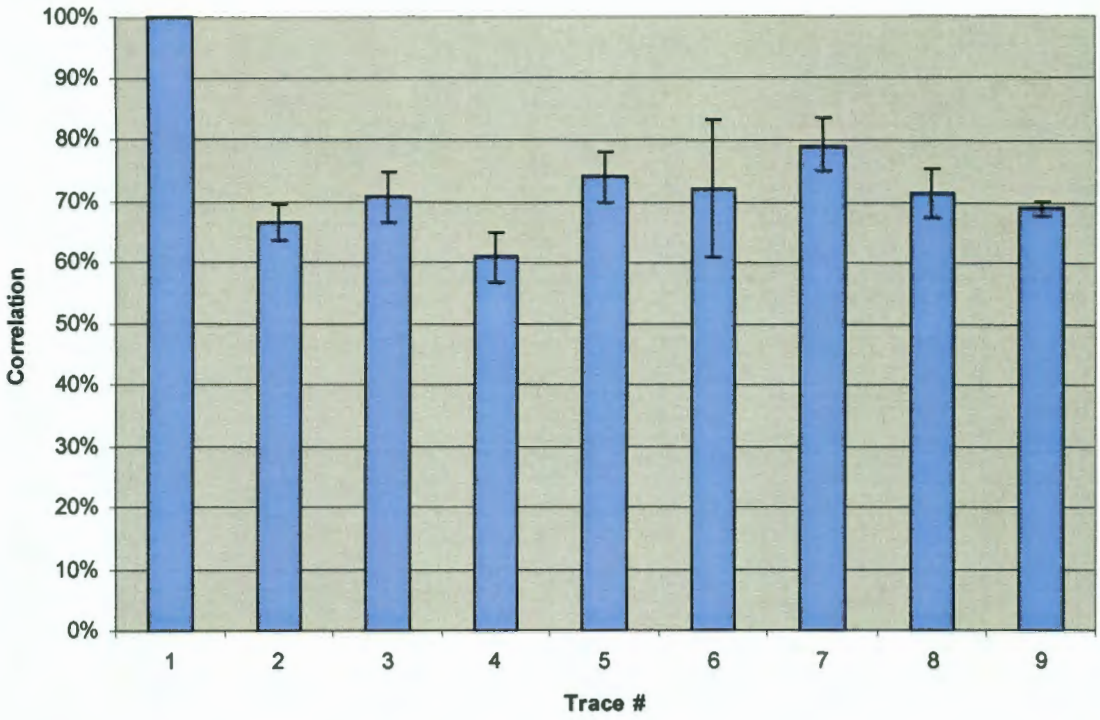


Trace #	Positions of the Endevco Model ex the Baseplate				
	Position 1 (18" from center)	Position 2 (14.25")	Position 3 (10.5")	Position 4 (6.5")	Position 5 (0")
5: Ground Force (Endevco Baseplate and Mass Acc.)	87.44%	95.10%	93.61%	92.62%	94.98%
6: Endevco Baseplate Acc.	86.93%	96.18%	95.92%	96.73%	84.18%

Figure 42. Correlation with the 28 Hz geophone and the Endevco accelerometer located on the baseplate reveals that placement makes a difference in signal response. Position 4 yields the best response.

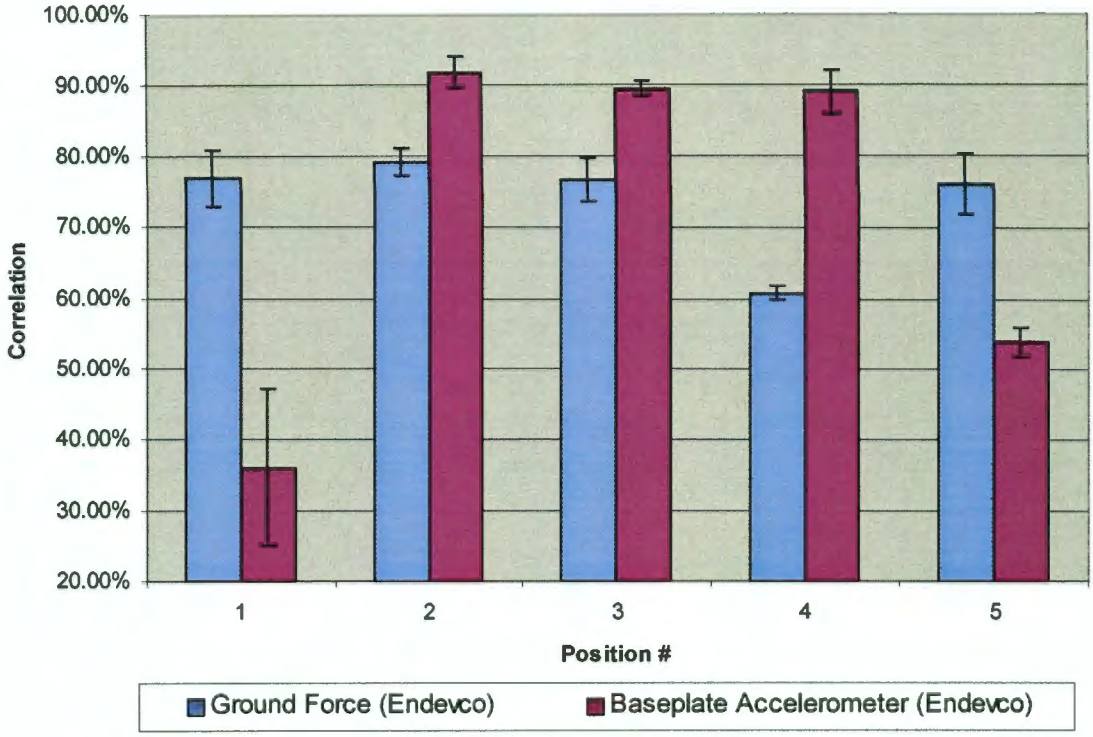
300-400 Hz

Next, a band pass filter (300-320-400-420) was applied (Figure 43). Again, the Endevco baseplate accelerometer is most similar to the 28 Hz geophone if placed at position 2 (91.88% ± 2%) (Figure 44). Moreover, position 3 (89.6% ± 1%) and position 4 (89.04% ± 3%) are very close in value to position 2. The drop-off in signal measurement at the rim and center of the baseplate is still predominant. It should also be noted that a major difference in this frequency range is that correlation coefficient significantly decrease.



Trace #	Correlation with Trace 1
1: 28 Hz Buried Geophone	100%
2: Ground Force (Dytran Baseplate and Mass Acc.)	66.59%
3: Dytran Baseplate Acc.	70.71%
4: Dytran Mass Acc.	60.83%
5: Ground Force (Endevco Baseplate and Mass Acc.)	73.98%
6: Endevco Baseplate Acc.	72.07%
7: Endevco Mass Acc.	79.14%
8: Sweep	71.38%
9: Pilot	69.02%

Figure 43. Correlation with the 28 Hz phone reveals that the Endevco mass accelerometer yields the highest fidelity of ground response.



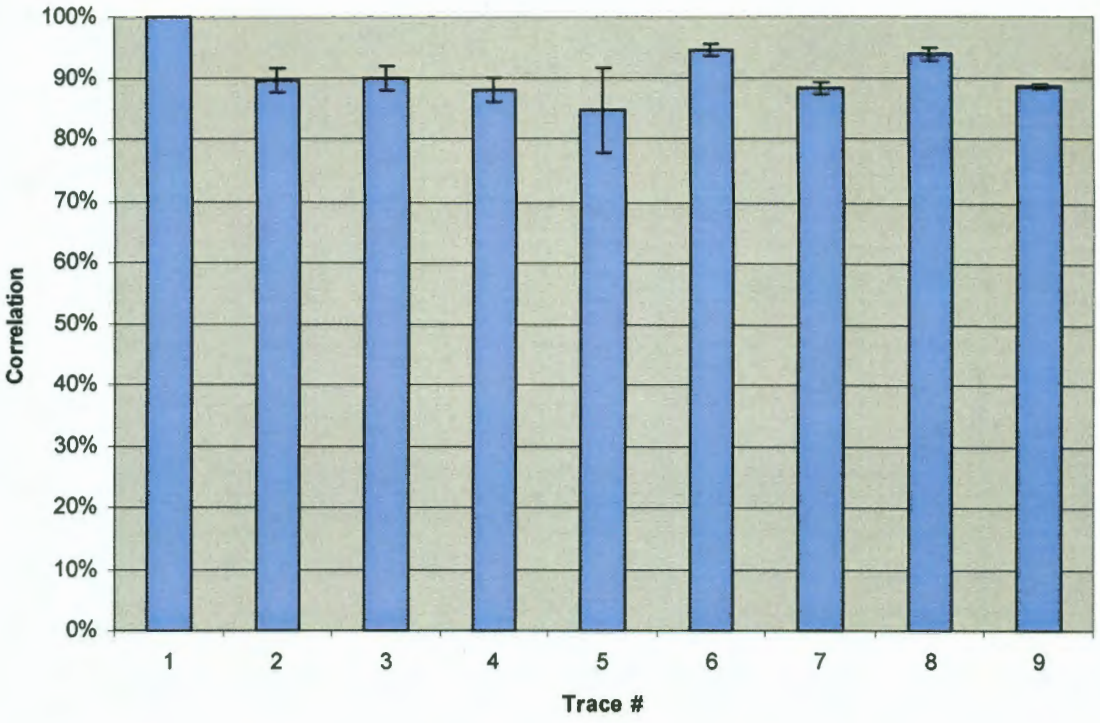
Trace #	Positions of the Endevco Model on the Baseplate				
	Position 1 (18" from center)	Position 2 (14.25")	Position 3 (10.5")	Position 4 (6.5")	Position 5 (0")
5: Ground Force (Endevco Baseplate and Mass Acc.)	77.00%	79.15%	76.75%	60.79%	76.22%
6: Endevco Baseplate Acc.	36.01%	91.88%	89.60%	89.04%	53.80%

Figure 44. Correlation with the 28 Hz geophone and the Endevco accelerometer located on the baseplate reveals that placement makes a difference in signal response. Position 2 yields the best response.

400-500 Hz

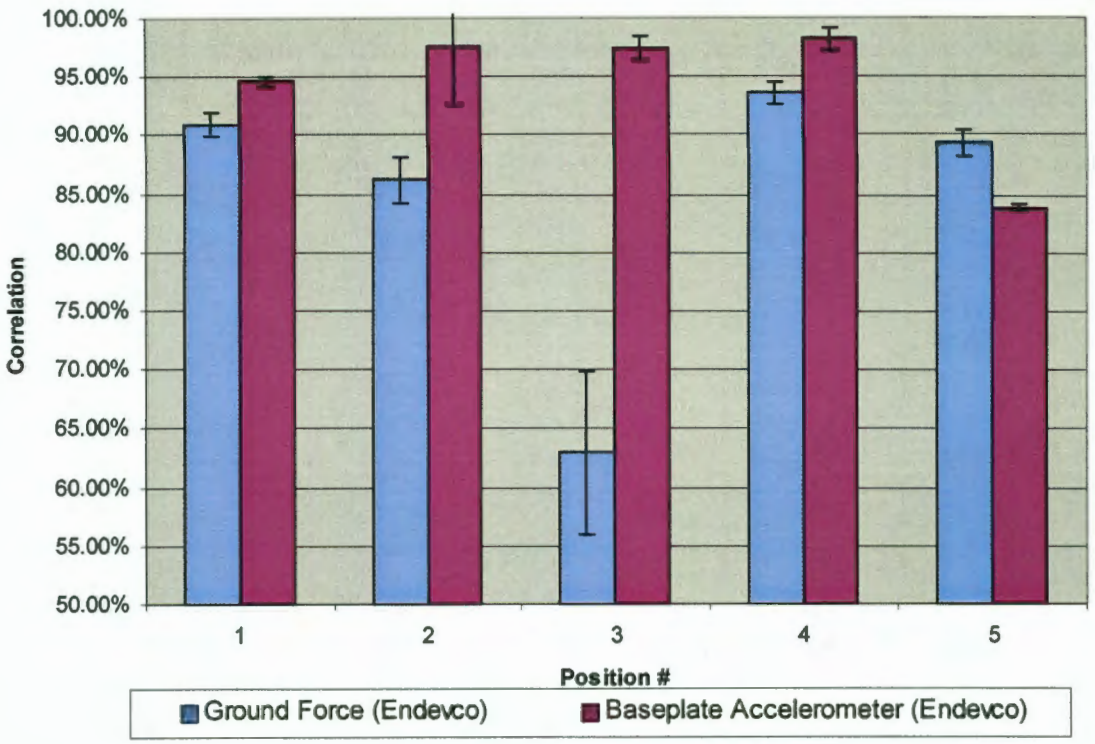
Finally, a band pass filter (300-320-400-420) was applied (Figure 45). Again, the Endevco baseplate accelerometer measurement is most similar to the 28 Hz geophone if placed at position 4 (98.22% ± 1%) (Figure 46). Moreover, position 2 (97.57% ± 5%) and position 3 (97.45% ± 1%) are very close in value to position 4. It should be noted that there is a significant drop-off in signal measurement at the rim and center of the baseplate. Also, correlation of the ground force with the baseplate accelerometer at position 3 yielded significantly lower values. Further analysis reveals no change in data quality, and that the correlation percentages varied from 74% to 54%, which explains the large standard deviation.

The computer program used to record the Dytran accelerometer measurements has a self-generating uncontrollable high-amplitude noise component that starts at 415 Hz and peaks at 600 Hz. While the cause of this is unknown, it appears not to impact the data.



Trace #	Correlation with Trace 1
1: 28 Hz Buried Geophone	100%
2: Ground Force (Dytran Baseplate and Mass Acc.)	89.61%
3: Dytran Baseplate Acc.	89.95%
4: Dytran Mass Acc.	87.99%
5: Ground Force (Endevco Baseplate and Mass Acc.)	84.62%
6: Endevco Baseplate Acc.	94.36%
7: Endevco Mass Acc.	88.13%
8: Sweep	93.88%
9: Pilot	88.53%

Figure 45. Correlation with the 28 Hz phone reveals that the Endevco baseplate accelerometer yields the highest fidelity of ground response.



Trace #	Positions of the Endevco Model on the Baseplate				
	Position 1 (18" from center)	Position 2 (14.25")	Position 3 (10.5")	Position 4 (6.5")	Position 5 (0")
5: Ground Force (Endevco Baseplate and Mass Acc.)	90.96%	86.25%	62.94%	93.60%	89.36%
6: Endevco Baseplate Acc.	94.62%	97.57%	97.45%	98.22%	83.96%

Figure 46. Correlation with the 28 Hz geophone and the Endevco accelerometer located on the baseplate reveals that placement makes a difference in signal response. Position 4 yields the best response.

Geophone Response

Far field results need to be discussed as well. Two major factors that cause attenuation of the seismic signal are spherical divergence and absorption (Figure 47). Signal attenuation due to spherical divergence is $1/r^2$ where, r represents the distance from a source to a receiver, and is measurable when absorption is low. However, near field measurements are difficult to make because absorption is high (Figure 48). Absorption is dependent on the medium in which the wave is propagating, so its effects are seen throughout a seismic record (Hatherly, 1986). Deconvolution of the geophones with the Endevco accelerometer produce a seismic record that is extremely detailed (Figure 49). First arrivals are predominant between 20 to 40 ms. Multiples may be present in the data set, which can make interpretation difficult. Reflection coefficients can contain complex values that phase shift the wavelets (Ulrych and Walker, 1982). Also, non-linear resonances are most likely present in the data due to a relatively high drive amplitude (Walker, 1995). As the drive amplitude increases chaotic energy increases and indicates a high energy state in the system. Wind noise may also have been a factor during the survey because it was steadily between 5 to 10 mph.

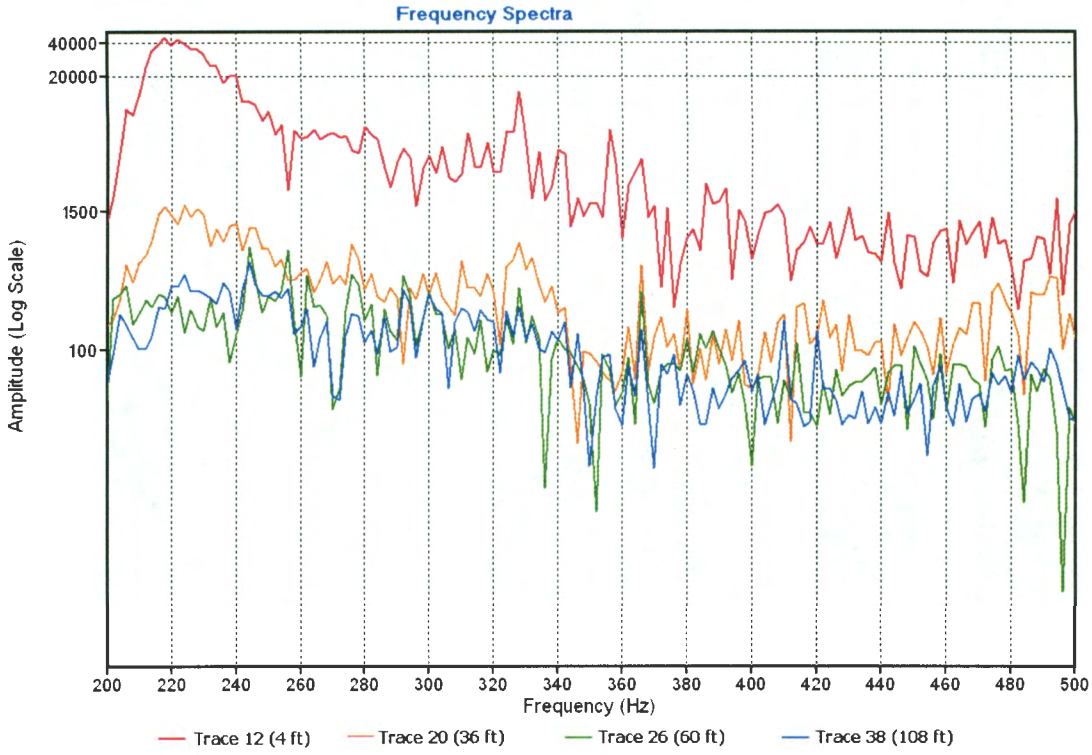


Figure 47. The frequency spectra reveal how amplitude will attenuate with distance.

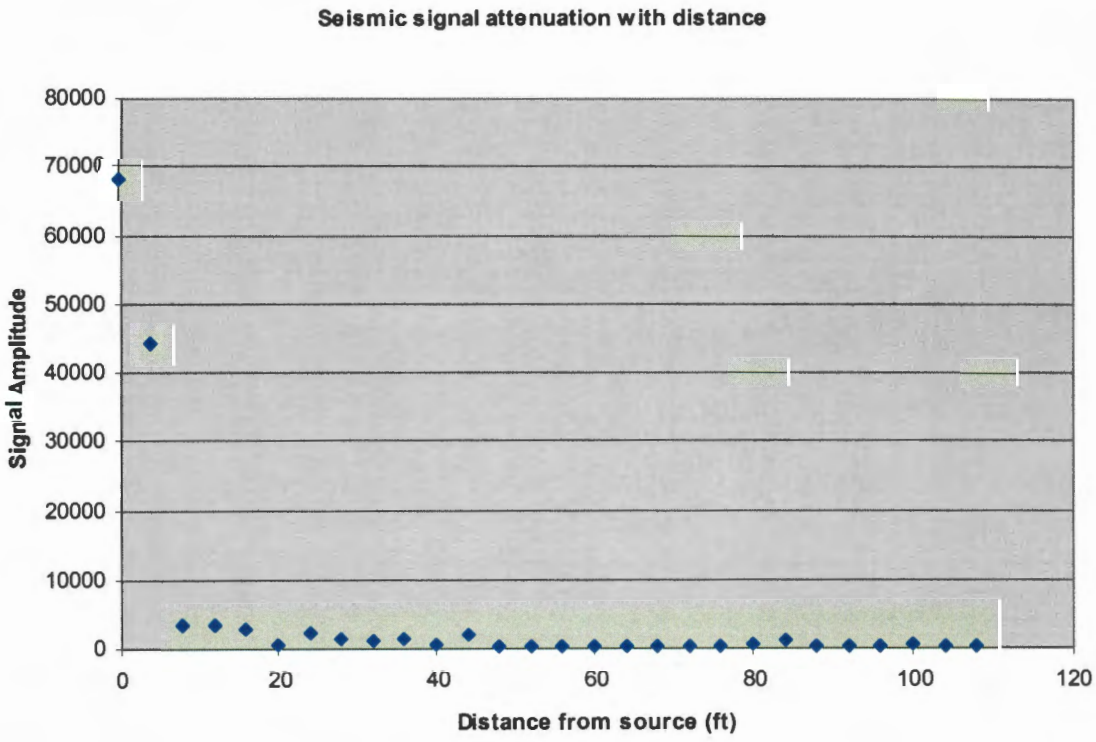


Figure 48. Graph depicting signal attenuation. The dropoff at near field distances is closer to $1/r^3$, which is due to absorption.

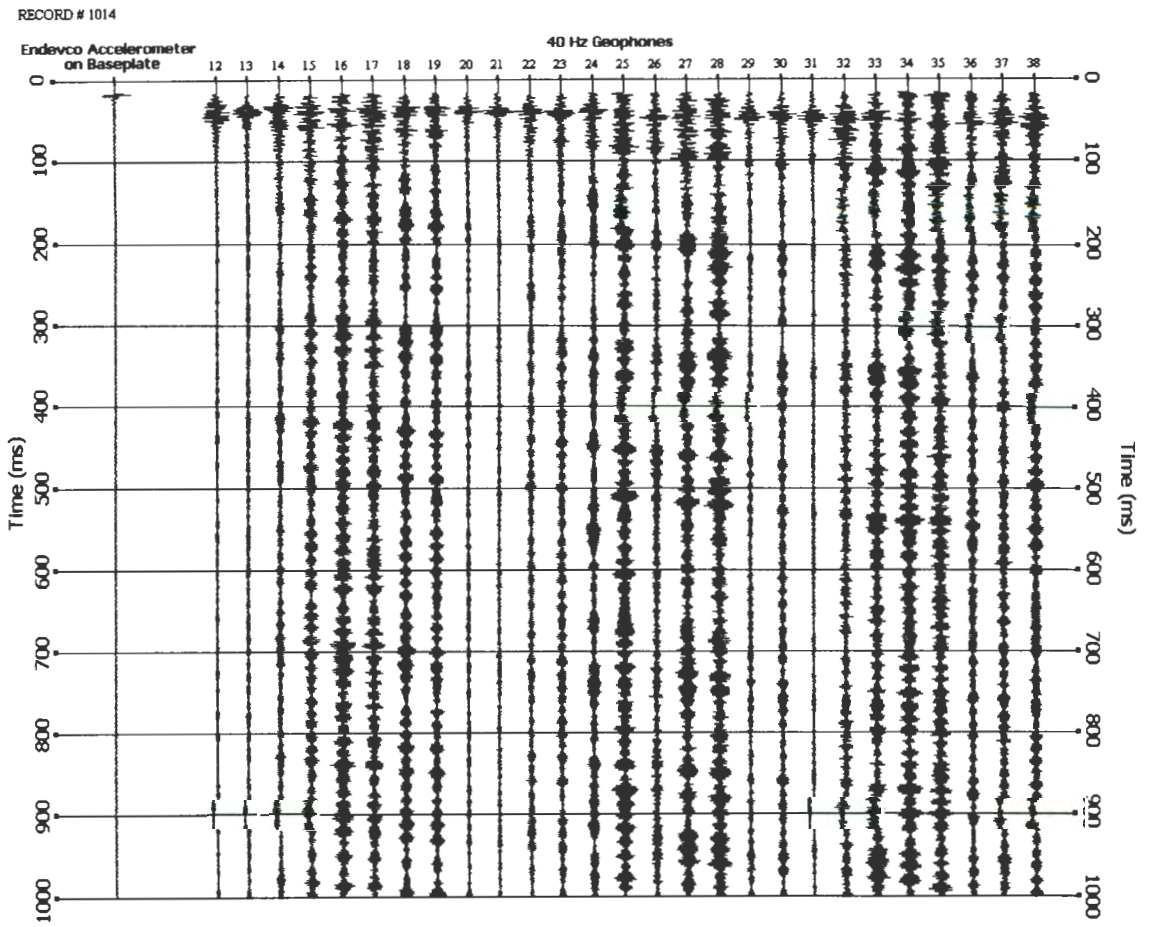


Figure 49. Deconvolution of the data set with the Endevco accelerometer at Position 4.

Conclusion

High-frequency vibroseis data can be improved by upgrading to higher-quality accelerometers, using good positioning of them on the baseplate, and processing data to reduce noise associated with the telemetry system. The IVI radio signal used to telemetry vibrator response contains noise and should not be used for correlation. Because deconvolution is frequency dependent, this is the suggested method for the telemetry signal. However, since deconvolution is also sensitive to noise, equipment with low noise threshold values should be used. The Endevco accelerometer is proved to be a significant improvement in data measurement and S/N. Accelerometer location on the baseplate also turned out to be a factor in true ground force measurements. For frequency ranges below 250 Hz, Position 3 is ideal. Above 200 Hz, Position 4 yielded the best performance although Position 2 and 3 will produce similar values. However, in every case, the accelerometer measured poorly in the positions on the rim and on top of the column. Interestingly enough, using the baseplate accelerometer alone gives the best measurement of true source signal. Analysis of geophone response shows that signal attenuates with distance due to spherical divergence and absorption of the seismic wave.

Some suggestions for surveys include using the Endevco accelerometer instead of the Dytran. For frequencies between 20-250 Hz, the accelerometer should be placed at position 3, and for higher frequencies sweeps, such as 200-500 Hz, the accelerometer should be located at position 4. The reaction mass accelerometer did not prove to be necessary in representing ground motion. The computer program that is currently used in the vibrator should not be used for higher frequencies because of an amplitude increase in the frequency spectra that starts at 415 Hz and peaks at 600 Hz. Future work on this

subject should examine the data set, including multiple reflections. Harmonics should also be studied with in the accelerometer recorded traces.

References

Allen, K.P, M.L. Johnson, J.S. May, Mobil E & P Technical Center, 1998. High fidelity vibratory seismic (HFVS) method for acquiring seismic data. SEG Expanded Abstracts.

Anstey, N.A., 1966. Correlation techniques - A review. *Journal of the Canadian Society of Expoloration Geophysicists*, **2**, p. 55-86.

Baeten, G., and A. Ziolkowski, 1990. *The Vibroseis Source.* Elsevier Science Publishers B.V., The Netherlands.

Ball, S.M., M.M. Ball, and D.J. Laughlin, 1963. Geology of Franklin County, Kansas: Kansas Geological Survey, Bulletin 163, p. 57.

Bickel, S.H., 1982. The effects of noise on minimum-phase Vibroseis deconvolution. *Geophysics*, **47**, p.1174-1184.

Brittle K.F., L.R. Lines, and A.K. Dey, 2001. Vibroseis deconvolution: a comparison of cross-correlation and frequency-domain sweep deconvolution. *Geophysical Prospecting*, **49**, p. 675-686.

Brook, R.A., and G.A. Crews, 1991. Experimental analysis of vibrator baseplate dynamics. SEG Technical Program Expanded Abstracts. p. 743-746.

Chapman, W.L., G.L. Brown, and D.W. Fair, 1981. The Vibroseis system: A high-frequency tool. *Geophysics*, **46**, p. 1657-1666.

Collins, F., and C.C. Lee, 1956. Seismic wave attenuation characteristics from pulse experiments. *Geophysics*, **21**, p. 16-40.

Edelmann, H.A.K., and H. Werner, 1982. The encoded sweep technique for Vibroseis. *Geophysics*, **47**, p. 809-818.

Futterman, W.I., 1962. Dispersive wave bodies. *Journal of Geophysical Research*, **67**, p. 5279-5291.

Geometrics, Cited in 2006. ftp://geom.geometrics.com/pub/seismic/DataSheets/NZ7.pdf

Hatherly, P.J., Attenuation measurements on shallow seismic refraction data. *Geophysics*, **51**, p. 250-254.

Hsueh, A.C., and J.M. Mendel, 1983. Maximum-likelihood vibroseis deconvolution. SEG Technical Program Expanded Abstracts, p. 363-365.

Industrial Vehicles International, Inc. (IVI), Cited in 2006. A seismic source radio trigger system. http://www.nacse.org/neesSiteSpecs/incoming/31/equipmentDoc/128/363/rts100m-98.pdf

Klemperer, S.L., and L. Brown, 1985. Simulations of noise rejection and mantissa-only recording: An experiment in high-amplitude noise reduction with COCORP data. *Geophysics*, **50**, p. 709-714.

Klimentos, T., and C. McCann, 1990. Relationships among compressional wave attenuation, porosity, clay content, and permeability in sandstones. *Geophysics*, **55**, p. 998-1014.

Lebedev, A.V., and I.A. Beresnev, 2004. Nonlinear distortion of signals radiated by vibroseis sources. *Geophysics*, **69**, p. 968-977.

Levin, F.K., 1979. Seismic velocities in transversely isotropic media. *Geophysics*, **44**, p. 918-936.

Lines, L.R. and T.J. Ulrych, 1977. The old and the new in seismic deconvolution and wavelet estimation. *Geophysical Prospecting*, **25**, p. 512-540.

Marschall, R., and M. Knecht, 1986. Reflectivity-corrected deconvolution and its influence on inversion. Research Workshop on Deconvolution and Inversion, 3-5 September 1986, Rome, Italy.

Miller, R.D., T.R. Rademacker, and J.L. Lambrecht, 2004. Field test of two high frequency vibrators with two high frequency servovalves at two sites in Kansas with near-surface emphasis. Presented at Society of Exploration Geophysicists, Denver, CO.

Rademacker, T.R., R.D. Miller, J. Xia, R. Black, G. Tsoflias, 2005. Enhancing the vibroseis technique through equipment noise reduction and optimizing the ground force signal. Presented at Society of Exploration Geophysicists, Houston, TX.

Robinson, E.A., 1967. Predictive decomposition of time series with applications to seismic exploration. *Geophysics*, **32**, p. 418-484.

Robinson, E.A., and M. Saggaf, 2001. Klauder wavelet removal before vibroseis deconvolution. *Geophysical Prospecting*, **49**, p. 335-340.

Robinson, E.A., S. Treital, 2000. *Geophysical Signal Analysis*. Society of Exploration Geophysicists, Tulsa. (Reprint of the 1980 edition.)

Sallas, J.J., 1984. Seismic vibrator control and the downgoing *P*-wave. *Geophysics*, **49**, p. 732-740.

Schrodt, J.K., L.H. Kumamoto, and Sohio Petroleum Co., 1985. New developments in Vibroseis technology. SEG Expanded Abstracts, **4**, p. 517-519.

Schrodt, J.K., 1987. Techniques for improving Vibroseis data. *Geophysics*, **52**, p. 469-482.

Seriff, A.J., and W.H. Kim, 1970. The effect of harmonic distortion in the use of vibratory surface souces. *Geophysics*, **35**, p. 234-246.

Serway, R.A., and R.J. Beichner, 2000. *Physics For Scientists and Engineers*. Saunders College Publishing, 5th Edition.

Ulrych, T.J., and C. Walker, 1982. Analytic minimum entropy deconvolution. *Geophysics*, **47**, p. 1295-1302.

VHF and UHF Characteristics, what to expect from each band, Cited in 2006. http://www.hamuniverse.com/vhfuhfbands.html

Vossen, R.V., A. Curtis, and J. Trampert, 2005. Subsonic near-surface P-velocity and low S-velocity observations using propagator inversion. *Geophysics*, **70**, p. R15-R23.

Walker, D., 1995. Harmonis resonance structure and chaotic dynamics in the earth-vibrator system. *Geophysical Prospecting*, **43**, p. 487-507.

Wuenschel, P., 1965. Dispersive body waves: an experimental study. *Geophysics*, **30**, p. 539-551.

Yilmaz, O., 2001. *Seismic Data Analysis*. Society of Exploration Geophysicists, 2nd Edition.

Appendix A:

The convolutional model for a vibroseis seismic source (Brittle et al., 2001):

$$x(t) = r(t)*s(t)$$

where x(t) is the recorded trace, r(t) is the reflectivity, s(t) represents the sweep, and all values are time dependent. * is the convolution operator. Removing the sweep involves cross-correlation, ⊗, with the sweep:

$$x_{cc}(t) = r(t)*s(t)\otimes s(t) = r(t)*k(t)$$

where k(t) is the Klauder wavelet.

Deconvolution uses the frequency domain so the equation for the convolutional model can be rewritten as:

$$X(\omega) = R(\omega)S(\omega)$$

This allows the sweep to be removed through division:

$$X(\omega)/S(\omega) = R(\omega)$$

Appendix B:

The equation of motion for a rigid body baseplate and reaction mass system is (Saïas, 1984):

$$F_t - F_g = M_r a_r + M_b a_b$$

where the force due to vehicle vibration, F_t $\begin{cases} = 0 \text{ if vehicle is vibrationally isolated} \\ \neq 0 \text{ if vehicle is not vibrationally isolated} \end{cases}$

F_g is the ground force, M_r is the reaction mass, a_r is the acceleration of the reaction mass, M_b is the mass of the baseplate and a_b is the baseplate acceleration.

Adding an addition spring system allows contact rigidity to be accounted for. Restoring force, F_c, is calculated (Lebedev et al., 2004):

$$M_g a_g + D_g v_g + K_g x_g = F_g + F_a(t)$$

Where M_g, D_g, and K_g are mass, dashpot and spring constant values associated with ground reaction. The actuator force, $F_a(t) = \sin\omega t$, and ω is the vibrator's operating frequency.